2397

JOHNSON

SANDIA REPORT SAND81-0629 • Unlimited Release
Printed October 1981

RECORD COPY
DO NOT TAKE FROM THIS ROOM

Thermo-Mechanical Scoping Calculations for a High Level Nuclear Waste Repository in Tuff

Roy L. Johnson

Prepared by
Sandia National Laboratories
Albuquerque, New Mexico 87185 and Livermore, California 94550
for the United States Department of Energy
under Contract DE-AC04-76DP00789

Issued by Sandia National Laboratories, operated for the United States Department of Energy by Sandia Corporation.
NOTICE: This report was prepared as an account of work sponsored by an agency of the United States Government. Neither the United States Government nor any agency thereof, nor any of their employees, nor any of their contractors, subcontractors, or their employees, makes any warranty, express or implied, or assumes any legal liability or responsibility for the accuracy, completeness, or usefulness of any information, apparatus, product, or process disclosed, or represents that its use would not infringe privately owned rights. Reference herein to any specific commercial product, process, or service by trade name, trademark, manufacturer, or otherwise, does not necessarily constitute or imply its endorsement, recommendation, or favoring by the United States Government, any agency thereof or any of their contractors or subcontractors. The views and opinions expressed herein do not necessarily state or reflect those of the United States Government, any agency thereof or any of their contractors or subcontractors.

SAND81-0629

THERMO-MECHANICAL SCOPING CALCULATIONS FOR A HIGH LEVEL NUCLEAR WASTE REPOSITORY IN TUFF*

Roy L. Johnson
Applied Mechanics Division II 5522
Sandia National Laboratories**
Albuquerque, NM 87185

October 1981

Abstract

Thermal and mechanical stress scoping calculations have been completed for a high level nuclear waste repository sited in welded tuff below the water table at the Nevada Test Site. Reported are the results of the studies performed at Sandia National Laboratories. A ubiquitous jointed rock model which allows slip along randomly oriented joints and subsequent stress redistribution due to slip and fracture of intact rock was used to model the rock mass. Computations were made for two power input levels and for conditions of boiling of the groundwater at 100°C and for no boiling of the groundwater.

* This work was supported by the U. S. Department of Energy (DOE) under Contract DE-AC094-76DP00789.

** A U. S. Department of Energy Facility.

Contents

	Page
INTRODUCTION	5
PROBLEM SPECIFICATIONS	6
Room and Pillar Geometry	6
Material Properties	6
Failure Criteria	8
FINITE ELEMENT ANALYSIS	12
Finite Element Mesh	12
Thermal Analysis	12
Stress Analysis	14
DISCUSSION OF RESULTS	18
Effects of Excavation	18
Effects of a Gross Thermal Loading of 75 kW/Acre	19
Effects of a Gross Thermal Loading of 100 kW/Acre	21
SUMMARY AND CONCLUSIONS	24
ACKNOWLEDGMENTS	26
REFERENCES	27
FIGURES 1 - 51	28, 77

INTRODUCTION

Summarized in this report are results of thermal and mechanical scoping calculations for a typical room and pillar configuration of a high level waste (HLW) repository in tuff. In all, four separate calculations were performed for gross thermal loadings (GTL) of 75 and 100 kW/Acre, each done for conditions of boiling of groundwater at 100°C and for no boiling of the groundwater. These calculations were performed for the Tuff Mine Design Study (MIDES) working group during FY80. The major portion of these results were previously reported in Reference [1].

A ubiquitous jointed rock model [3] which allows slip along randomly oriented joints and subsequent stress redistribution was used to model the rock mass. A fracture criterion was employed to detect failure of intact rock between joints. Three post-failure mechanisms were considered in the analysis: 1) failure in shear along two planes making equal angles with the direction of minimum principal stress; 2) brittle splitting along lines of minimum principal stress; and 3) rubblization of the material between joints.

Calculations were performed using the 1978 version of the computer codes ADINAT [4] and ADINA [5]. A material model for jointed rock and a fracture initiation criterion for failure of intact rock was added to ADINA for the purpose of performing these calculations.

PROBLEM SPECIFICATIONS

The problem description for these calculations, including the design geometry to be analyzed and the thermal and mechanical material properties, were specified by the MIDES Working Group [2]. They are summarized in this section of the report.

Room and Pillar Geometry

A half-section of the room and pillar with pertinent dimensions is shown in Figure 1. Excavation of the room to these dimensions results in a horizontal extraction ratio of 0.20 (2.5 m/12.5 m). For stress calculations the waste emplacement hole is assumed to have the same mechanical properties as the surrounding tuff.

Material Properties

Thermal calculations were based on the relative heat generation decay properties of high level waste (HLW) as listed in Table 1. Thermal properties of each of the component materials are shown in Table 2. The tabulated values of conductivity and specific heat for tuff are based on the condition of no boiling of the groundwater. If boiling conditions exist then the variation with temperature of conductivity and specific heat are assumed to be as shown in Figure 2.

TABLE 1

RELATIVE HEAT-GENERATION DECAY PROPERTIES[a]

Year After Emplacement[b]	HLW
0	1.0
1	.95
2	.907
3	.871
4	.851
5	.810
6	.783
7	.769
8	.734
9	.714
10	.692
15	.600
20	.529
30	.402
40	.313
50	.246
70	.157
100	.0864
190	.0296
290	.0215
390	.0163
490	.0145
590	.0127
690	.0113
790	.0100
890	.00897
990	.00810
1990	.00404
5990	.00230
9990	.00175

[a]See Y/OWI/TM-34, "Nuclear Waste Projections and Source Term Data for FY 1977." The HLW decay rates correspond to waste arising from fuel which is a 3:1 mix of fresh UO_2 and MOX fuels.

[b]Assumes waste is 10 years old at emplacement.

Table 2.

THERMAL PROPERTIES

MATERIAL	CONDUCTIVITY Joules/Yr-m-°C	SPECIFIC HEAT Joules/m^3-°C
Vol. Heat Source	3.82×10^7	2.51×10^6
Tunnel Radiation	7.88×10^6	1.0×10^3
Tuff (Noboil)	7.57×10^7	3.64×10^6

Mechanical properties of intact rock and the jointed rock mass are listed in Tables 3 and 4. Joint orientation angles are computed using a random function which allows dispersion about a mean joint angle specified here as 90 degrees. No information was available on dispersivity of joint angles, therefore a joint angle dispersion coefficient $K = 10^6$ was used in these calculations. This results in a joint orientation which is essentially vertical.

Rock strengths are based on saturated conditions.

Failure Criteria

Coulomb-type failure criteria are used to detect initiation of slip along pre-existing joints, and for initiation of intact rock failure. The criteria are illustrated in Figure 3. Effective stress, $\bar{\sigma}_j$, for joint failure is the stress normal to the plane of the joint. The effective shear strength of the joint, τ, is then $\mu\bar{\sigma}_j$ where μ is the coefficient of joint friction. Slip occurs when the shear stress on the plane of the joint exceeds the strength.

The effective stress, $\bar{\sigma}_i$, for intact rock is taken as the mean stress, $(\sigma_{xx} + \sigma_{yy} + \sigma_{zz})/3$, where the interstitial pore pressure of the rock is not included. Failure occurs when the Mohr's circle representing a computed state of stress becomes tangent to the failure surface. The effective shear strength is given by

$$\tau = 8.5 + .93\bar{\sigma}_i$$

The stress state at each integration point of every element of the finite element mesh was examined for possible slip along joint planes and for intact rock failure. Failure of the intact rock was viewed as creating new joints in the rock up to a maximum of three, including the initial joint.

When a single new joint is created, as would happen by splitting along lines of minimum principal stress, subsequent behavior of the new joint is governed by the lower of the two curves shown in Figure 3. The technique for treating this mechanism is described in Reference [3]. When two new joints are created, such as when slip occurs along the two possible shearing failure planes, then the material is assumed to be a rubble, and its subsequent behavior is treated as that of an isotropic granular material.

TABLE 3.

MECHANICAL PROPERTIES INTACT ROCK
AS SPECIFIED IN REF. [2]

PROPERTY	TEMPERATURE 20°	99.99°	100.01°	1000°	UNITS
Young's Modulus	20.	20.	20.	20.	GPa
Poisson's Ratio	.25	.25	.25	.25	--
Shear Modulus	8.	8.	8.	8.	GPa
Coeff. Exp.	7.5×10^{-6}	7.5×10^{-6}	10.3×10^{-6}	10.3×10^{-6}	$°C^{-1}$
Coeff. Friction	.93	.93	.93	.93	--
Cohesion	8.5	8.5	8.5	8.5	MPa

TABLE 4.

MECHANICAL PROPERTIES JOINT BEHAVIOR
AS SPECIFIED IN REF. [2]

PROPERTY	TEMPERATURE 20°	99.99°	100.01°	1000°	UNITS
Coeff. Friction	.70	.70	.70	.70	--
Cohesion	.01	.01	.01	.01	MPa
Joint Angle	90°	90°	90°	90°	Degrees
Joint Angle Dispersion Coefficient	10^6	10^6	10^6	10^6	--

FINITE ELEMENT ANALYSIS

Finite Element Mesh

The thermal and mechanical analyses were performed using the same number of finite elements. A plot of the complete mesh and that of a portion of the mesh in the region of the room are shown in Figure 4.

The thermal mesh consisted of 498 nodal points and 446 four-node quadrilateral elements. Eight-node quadrilateral elements were used for stress calculations. Higher order elements were used to achieve better stress resolution close to the room in regions of high stress concentration. This refined mesh consisted of 1441 nodal points with the corner nodes of each element having the same spatial locations as those of the four-node elements.

Nodal point temperatures for the eight-node quadrilateral mesh were interpolated from those computed for the four-node quadrilateral mesh using the computer program MERLIN [6].

The order of numerical integration used to evaluate the element stiffness matrices was 2 x 2 for the four-node quadrilaterals and 3 x 3 for the eight-node quadrilaterals.

Thermal Analysis

The three-dimensional problem of a cylindrical heat source was reduced to a planar one by idealizing the waste canister as

an "equivalent" heat source having the dimensions of the canister hole in the plane but extending infinitely in the out-of-plane direction. This equivalent heat source is a function of gross thermal loading, canister power, canister hole dimensions, and canister pitch. Table 5 gives the values of equivalent heat sources used in the analyses.

Table 5.

Equivalent Heat Source

GTL kW/Acre	$\dot{Q}$ J/yr-m^{3}x10^9
75	13.1630
100	17.5507

The effects of radiation and convection within the room excavation were approximated by defining solid, conduction elements with appropriate properties. In Reference [7], O. L. George shows the importance of thermal radiation in determining temperatures around the periphery of the room and that this mechanism could be satisfactorily approximated by a thermal conduction model with a large diffusivity. In accordance with his recommendations, the following conduction properties were used in these studies for modeling room elements:

$$K = 7.88 \times 10^8 \text{ J/yr-m-°C}$$

$$\rho C_p = 1000. \text{ J/m}^3 \text{ - °C.}$$

Thermal calculations were performed using the computer code ADINAT [4]. A postprocessor POSADT2 was used to interface

Table 6.

PEAK TEMPERATURES
AT VARIOUS LOCATIONS

Temperatures in °C, Time in Years after Emplacement
Based on an Initial Temperature of 55°C

Node	Location	GTL = 75 kW/Acre				GTL = 100 kW/Acre			
		100°C Boil		No Boiling		100°C Boil		No Boiling	
		Temp.	Time	Temp.	Time	Temp.	Time	Temp.	Time
265	Centerline Room Floor	97	50	107	40	105	50	125	40
271	Lower Corner Room	97	50	107	40	105	50	125	40
276	Midheight Room Rib	96	50	106	40	104	50	124	40
281	Upper Corner Room	95	50	106	40	103	50	123	40
452	Centerline Room Roof	95	50	106	40	103	50	123	40
106	1/4 Pillar	94	75	105	50	100	75	121	40
102	Centerline Pillar	94	75	104	50	99	75	119	40
	Middepth Heat Source	145	10	144	12	177	7	168	12

output of ADINAT with existing plotting codes CNTR [8] and TPLOT2 [9] to produce the graphs of data shown in Figures 5-8 and 10-17.

Isotherms at times of 1, 5, 10, 50 and 100 years after emplacement of the waste are presented in Figures 5 through 8 for each of the four cases considered. Ambient temperature was taken as 55°C [2]. Plots of temperature vs. time at several locations around the room are shown in Figures 10 through 17. The locations of these points are shown in Figure 9.

Peak temperatures for various locations and the approximate times at which they occur are listed in Table 6. The no boiling cases produce the highest peak temperatures with the 100 kW/Acre GTL condition producing the highest of all cases considered.

Peak temperatures at points around the room occur at approximately 50 years for the 100°C boiling condition and at approximately 40 years for the no boiling condition.

The shape of the temperature vs. time plots are generally the same; however, it is noted that the slope of the curves after peak temperatures are reached is greater for the no boiling condition indicating a faster rate of cool down.

Stress Analysis

Results of the stress analysis calculations are presented graphically by the following plots:

1) Joint state indicators where an "X" is placed at an integration point where a joint or crack is closed and

slipping, with an "O" indicating that a joint or crack is open. Joint states are shown for a given time and are not cumulative.

2) Joint or crack orientations for pre-existing joints are displayed as vertical lines at each of four integration points within an element. Cracks caused by longitudinal splitting are indicated by lines through integration points in the direction of minimum principal stress (compression). Shear failures appear as two lines making equal angles with the direction of minimum principal stress. Cracks are displayed at each integration point where the intact rock failure criterion is satisfied.

3) Contours of equal horizontal or vertical stress. Contours are drawn at 5 Mpa intervals. A negative sign indicates compressive stress.

4) Plots of vertical displacement of the room floor and roof as a function of time.

Calculations were performed using a version of ADINA-78 modified to include the ubiquitous jointed rock material model [3].

In situ stresses were approximated by computing initial stresses for each element based on depth as follows:

$$\sigma_v = \text{Vertical Stress} = \rho g z$$

$$\sigma_h = \text{Horizontal Stress} = K\sigma_v$$

where z is measured from the ground surface to the depth of the point considered, ρ is the mass density of the overburden, and g is the acceleration of gravity. The factor K, the ratio of horizontal stress to vertical stress, was taken as [2]

$$K = 2.4 \qquad z < 100 \text{ m}$$

$$K = 0.4 + \frac{200}{Z} \qquad z \geq 100 \text{ m}$$

At the floor of the room, the depth, Z, is 800 m resulting in a value of K = 0.65.

Initial strains normal to the joint surfaces were computed using the initial stresses calculated above and a rock mass modulus of 2 GPa. These strains were then continuously monitored to determine the joint state - that is, whether the joint was closed or open. A small positive (tensile) stress or strain normal to the joint was interpreted as causing the joint to open. Initially all joints are assumed to be closed.

The effects of using a reduced modulus for computing initial joint strains was investigated. It was found that the use of an initial modulus of 20 GPa resulted in a larger zone of open joints in the room rib and pillar than that which was computed using the smaller rock mass modulus of 2 GPa. Conversely, fewer intact rock failures occurred when the

higher initial modulus was used. Vertical displacements of the room roof and floor were essentially unchanged.

From the viewpoint of mechanical behavior, it was felt that the solution obtained using the reduced initial modulus was conservative, hence it is these results which are presented here. Permeability studies might be more appropriately made using a higher initial modulus.

DISCUSSION OF RESULTS

General

Calculations were performed for a fixed room and pillar geometry. Effects of varying this geometry, such as changing fillet radius, and depth of burial of canister were not studied. In addition to neglecting the effects of interstitial pore pressures, the effect of drying of the rock due to boiling of the ground water and subsequent increase in strength of the dry rock was not considered.

Excavation of the room was handled in the computations by simultaneously "killing" all elements within the boundaries of the room. An excavation sequence was not considered, nor was any consideration given to the type of mining operation, such as drilling and blasting or use of a mining machine. If drilling and blasting operations are used the zone of rock failure could easily be of the same dimensions as those computed. Consequently, the localized failures discussed in the following sections may not actually represent failure zones created by excavation.

Effects of Excavation

Figure 18(a) shows that after excavation a region of the joint failure extends approximately 2.0 m into the pillar from the room rib. The failure mechanism is primarily slip along closed joints; however, some joints near the room rib are open.

No intact rock failure occurs as the result of room excavation as shown in Figure 18(b).

As shown in Figure 19, a maximum horizontal compressive stress of -20 MPa occurs in the bottom fillet where the room floor joins the rib. Vertical stresses of -35 MPa occur in the room rib just below and just above the top and bottom fillets of the room, respectively.

Effects of a Gross Thermal Loading of 75 kW/Acre

Figure 20 is a composite of plots of joint state indicators and joint and crack orientations at times of 1, 5, 10, 50 and 100 years after emplacement of the waste for a GTL of 75 kW/Acre where boiling of the groundwater is assumed to occur at 100°C. The first indication of intact rock failure occurs at 10 years. The mechanism of failure is splitting in both the upper and lower corner fillets of the room. This is followed by shear failures in the lower corner fillet at 50 years. No additional failures are indicated at 100 years.

The effects of temperature at early times is to decrease joint slip activity from that which occurred at time of excavation. At later times the zones of open joints extend farther into the pillar than the zone at time of excavation. For all cases considered, excavation causes the most severe perturbation of the stress fields. The effect of temperature at early times is to close joints due to thermal expansion while at later times, after peak temperatures have been reached, joints tend to open as the result of cooling.

Figures 21 through 25 are stress contour plots of horizontal and vertical stresses at times corresponding to those shown in Figure 20.

The effects of stress redistribution as the result of intact rock failure for this case is not clear. It can be seen from the stress contour plots that the location of maximum horizontal compressive stress shifts from the lower corner of the room to the upper corner at approximately 50 years. From Figure 20 it appears that this is the result of decrease in joint slip in the upper corner of the room at 50 years. Whereas joint slip in the lower corner is still occurring at 50 years and later.

Results of the no boiling condition for a GTL of 75 kW/Acre are shown in Figures 26 through 31. Joint activity patterns are similar to those of the boiling case. The first indication of intact rock failure is at 10 years with a shear failure initiated in the lower corner of the room and splitting occurring in the upper corner. The shear failure initiates splitting in an adjacent element in the lower corner while splitting remains the only mechanism of failure in the upper corner. Intact rock failures have stabilized at 100 years.

The location of the maximum horizontal compressive stress remains at the lower corner of the room for all times shown.

Effects of a Gross Thermal Loading of 100 kW/Acre

Figures 32 through 37 show results of the computations for a GTL of 100 kW/Acre where boiling of the groundwater occurs at 100°C. At later times the zone of open joints tends to extend around the corners of the room with fewer open joints occurring in the pillar.

The first intact rock failures occur at approximately 10 years with splitting at the upper and lower corners of the room. At later times shear failures occur at both locations with an extension of splitting into both the floor and roof of the room.

Intact rock failures are still occurring at 100 years, with the zone of splitting extending deeper into the floor at the corner of the room.

The maximum horizontal compressive stress initially is located at the lower corner of the room and remains there for all later times.

A significantly different pattern of joint activity is noticed in the plots of Figure 38 for the GTL of 100 kW/Acre and the no-boiling condition. Both joint slip and opening of joints occur farther into the pillar than for those of all other cases. The depth of the zone of joint failure is approximately 2.5 m. The zone is approximately triangular in shape and extends around both the upper and lower corners of the room.

Intact rock failures occur at approximately 5 years at both the lower and upper corners of the room. The initial mechanism is splitting which initiates shear failures in both the upper and lower corners of the room. At 50 years there is an indication of rubblization of the fillet at the lower corner of the room, with further extension of the zone of failure at 100 years, primarily in the floor of the room.

The effects of stress redistribution due to intact rock failure are apparent from the stress contour plots shown in Figures 39 through 43. There is a shift of maximum horizontal compressive stress from the lower corner to the upper corner of the room at approximately 50 years. At that time, the location of the maximum compressive stress has migrated from the surface of the lower corner fillet to a zone away from the surface. This can be explained by the fact that at this time the material of the fillet has crushed and no longer has strength other than that of an isotropic granular material. The location of competent rock is moved deeper into the corner of the room, in effect removing the fillet.

Displacements of the floor and the roof along the centerline of the room for GTL's of 75 kW/Acre and 100 kW/Acre are plotted in Figures 44 and 45, respectively. Displacements are plotted as functions of time after emplacement of the waste. The calculations show larger displacements for the no-boiling condition than for the boiling condition. For all cases the displacements are still increasing after 100 years.

The vertical room closure is indicated by the difference between the floor and roof displacement curves for each case. The fact that this difference remains fairly constant indicates that the displacement of the room follows the motion upward of the surrounding media caused by heating. The effects of stress redistribution do not significantly affect the room displacements. This is substantiated by the plots of displacements obtained from a linear elastic solution for an intact rock medium with a GTL of 100 kW/Acre and the no-boiling condition. The linear elastic model assumes no existing jointing of the rock mass and an infinite strength of the intact rock, thus no slip or intact rock failure with subsequent redistribution of stress occurs. Changes in stress distributions are functions only of the changes in temperature gradient. These displacements are superposed on the results of the nonlinear solution in Figure 45.

Results of stress distributions obtained from the linear solution are shown in Figures 46 through 51. It is noted that the zones of maximum compressive stress remain near the surfaces of the upper and lower corner fillets for all times.

SUMMARY AND CONCLUSIONS

Under the direction and guidance at the Nides Working Group, thermal and mechanical calculations were performed for a representative high level nuclear waste repository sited in tuff. Two power input levels were considered together with two conditions on behavior of the groundwater, those of boiling at 100°C and for no boiling.

Joint failure, interpreted as slip along existing vertical joints, is most prevalent after excavation of the room. The effects of temperature are to cause zones of open joints, especially in the pillar adjacent to the room rib, and to cause localized failure of intact rock in the corners of the room. The intact rock failures tend to stabilize between 50 and 100 years. The exception is the 100 kW/Acre GTL no boiling case where intact rock failures are still occurring at 100 years.

Displacements of the room increase monotonically up to 100 years and result in an essentially uniform upward motion of the room as the result of heating of the rock column. Room closure, the result of differential motion of the floor and roof of the room is approximately 0.5 cm.

Factors not considered in these analyses are:

1. Sensitivity to room fillet sizes.
2. Sensitivity to depth of burial of waste.
3. Effect of drying on rock strength.

4. Effects of a moving vaporization front and movement of groundwater.
5. Effects of excavation and rock bolting procedures.

Acknowledgments

The author would like to acknowledge the continuous discussions throughout this work with R. K. Thomas (5521), and the helpful review comments of K. W. Schuler (5521) and R. M. Zimmerman (4537).

References

1. Johnson, R. L., 2-D Room and Pillar Mechanical Scoping Calculations for HLW," Sandia National Laboratories, Letter Memorandum, July 1, 1980.

2. Mine Design Working Group - Activity Work Package, December 4-5, 1979.

3. Thomas, R. K., "A Material Constitutive Model for Jointed Rock Mass Behavior," SAND80-1418, November 1980.

4. Bathe, Klaus-Jurgen, "ADINAT: A Finite Element Program for Automatic Dynamic Incremental Nonlinear Analysis of Temperatures," Report 82448-5, Massachusetts Institute of Technology, May 1977 (Rev. Dec. 1978).

5. Bathe, Klaus-Jurgen, "ADINA: A Finite Element Program for Automatic Dynamic Incremental Nonlinear Analysis," Report 82448-1, Massachusetts Institute of Technology, September 1975. (Rev. Dec. 1978).

6. Gartling, David K., "MERLIN - A Computer Program to Transfer Data Between Finite Element Meshes," SAND81-0463, In Preparation.

7. Gartling, David K., Eaton, Roger R., and Thomas, Robert K., "Preliminary Thermal Analysis for a Nuclear Waste Repository in Tuff," SAND80-2813, April 1981.

8. Beisinger, Zelma E., and Benzley, Steven E., "Structural Mechanics Computer Plotting Handbook," SAND75-0038, September 1975.

9. Beisinger, Zelma E., and Stone, Charles M., "TPLOT2: A Flexible X-Y Plotting Program for Use with Finite Element Software," SAND80-2508, February 1981.

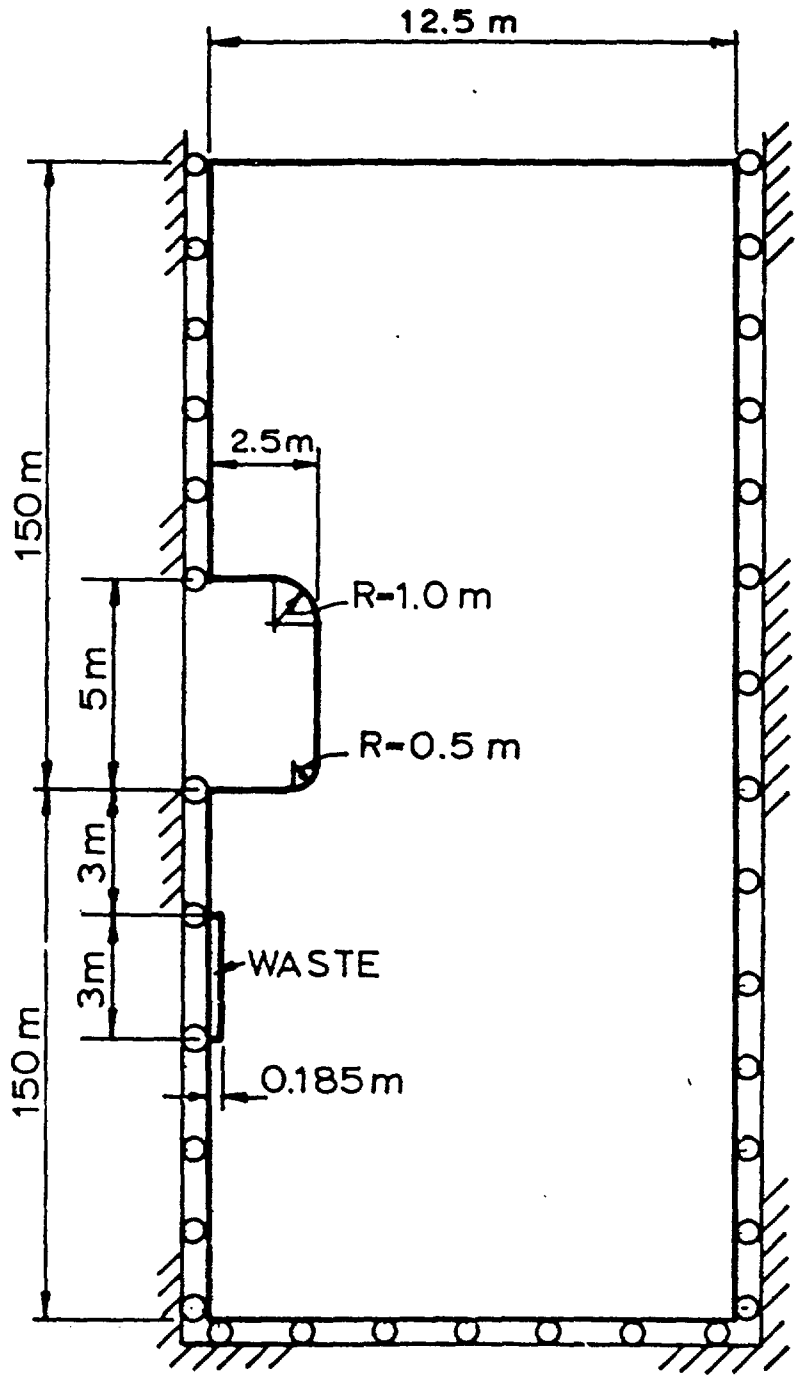

Figure 1. Half-Section of a Typical Room and Pillar for a High Level Waste Repository in Tuff.

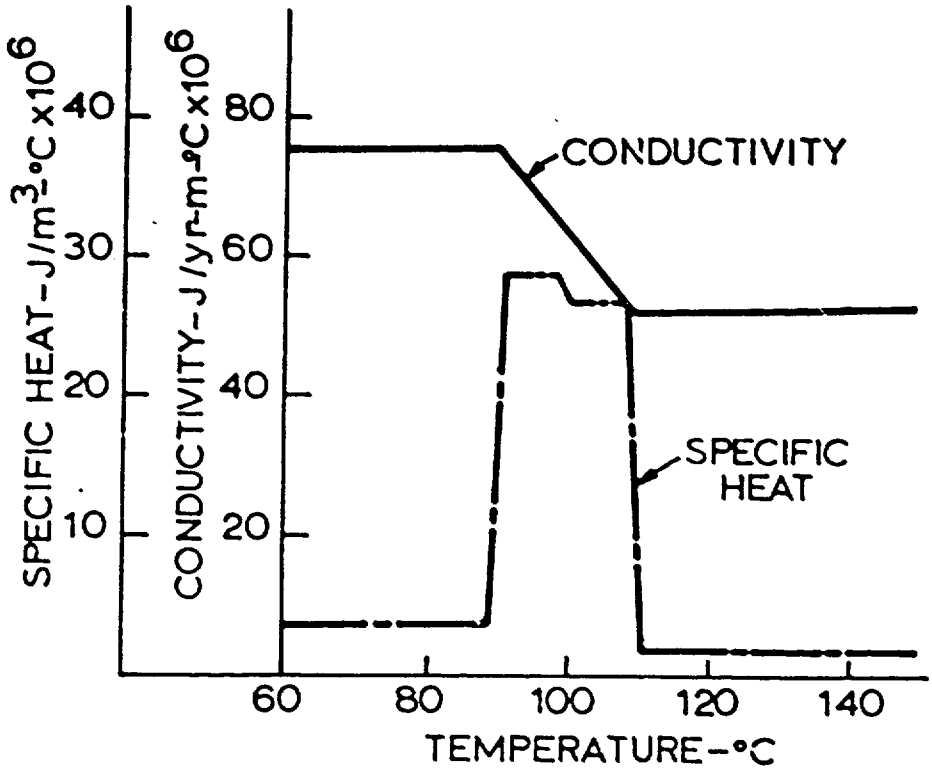

Figure 2. Variation of Thermal Conductivity and Specific Heat as a Function of Temperature for Tuff Assuming Boiling of the Groundwater at 100°C.

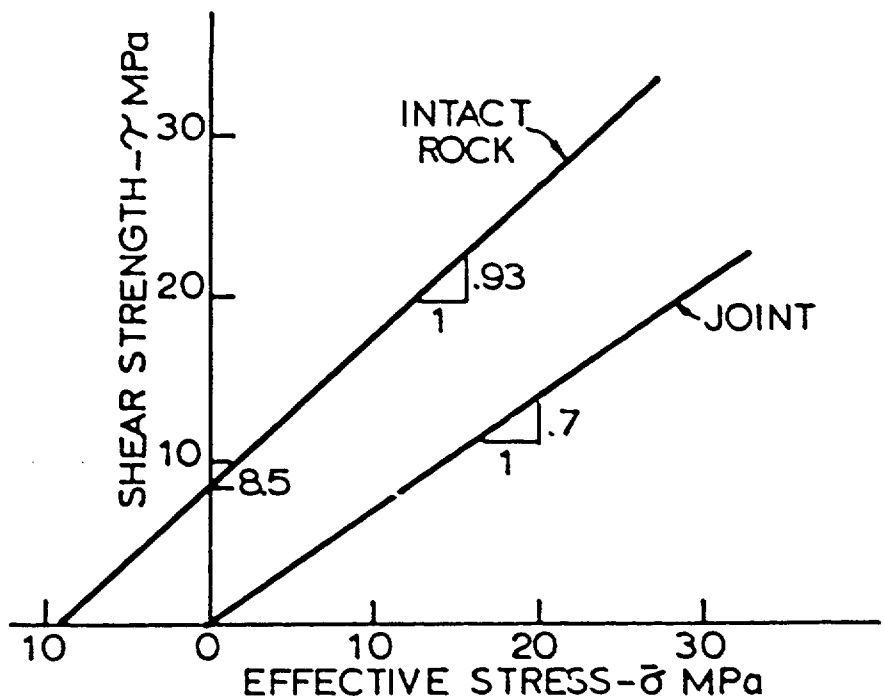

Figure 3. Coulomb Failure Surfaces for Jointed and Intact Rock Failure for Tuff.

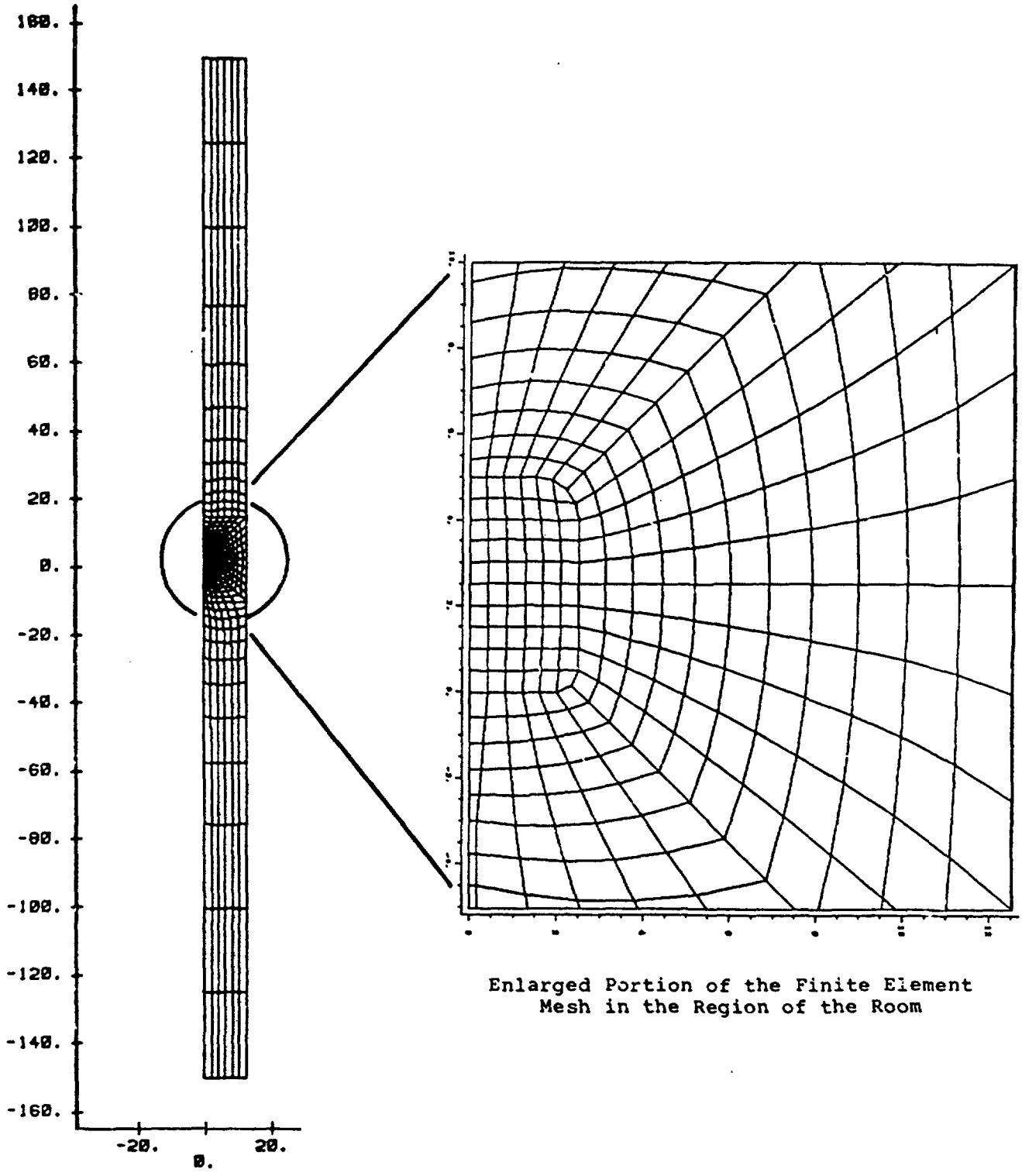

Enlarged Portion of the Finite Element Mesh in the Region of the Room

Figure 4. Finite Element Mesh Consisting of 446 Quadrilateral Elements Used to Discretize the Region of Figure 1.

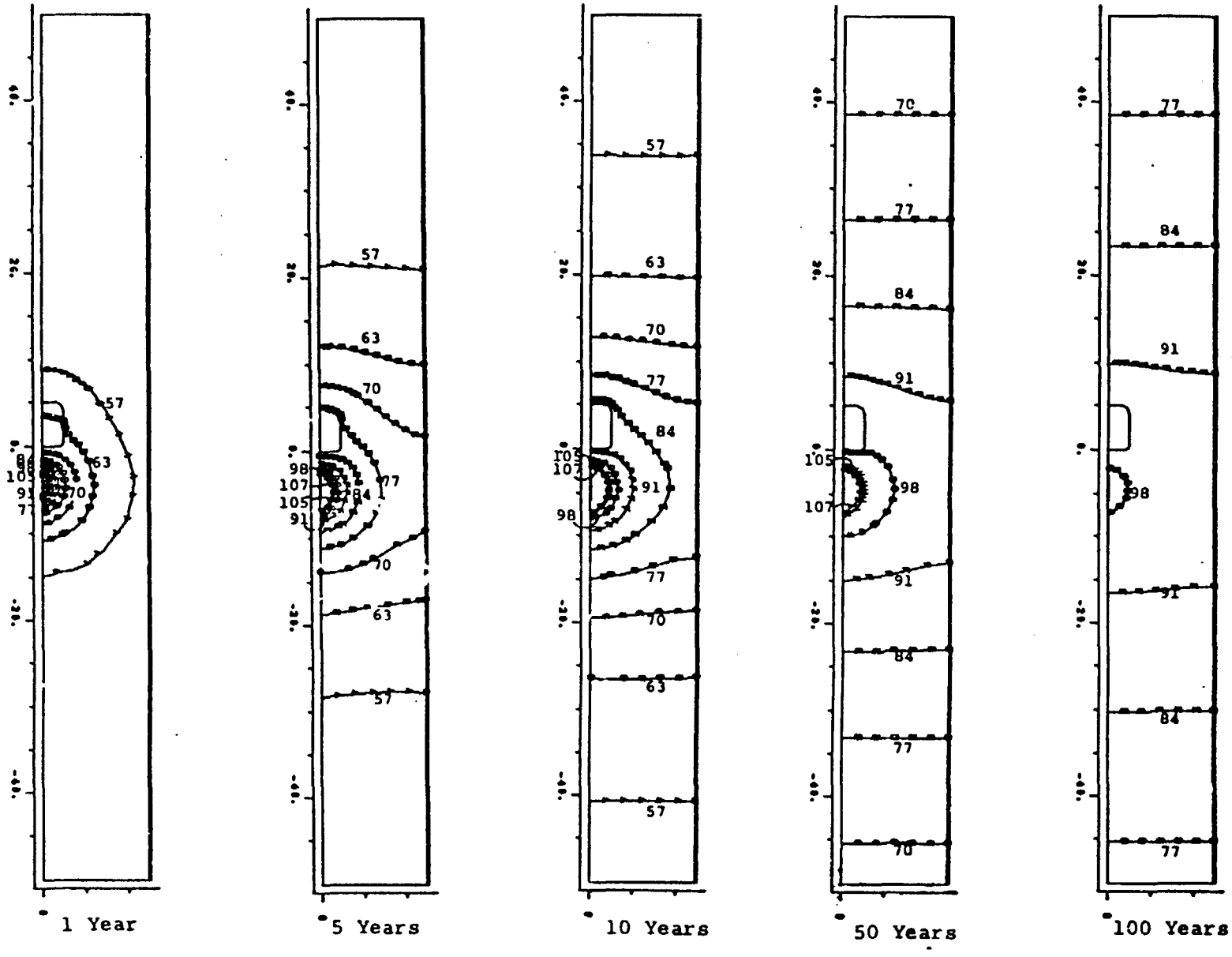

Figure 5. Isotherms at Various Times for HLW
GTL = 75 kw/A, 100°C Boiling of Groundwater

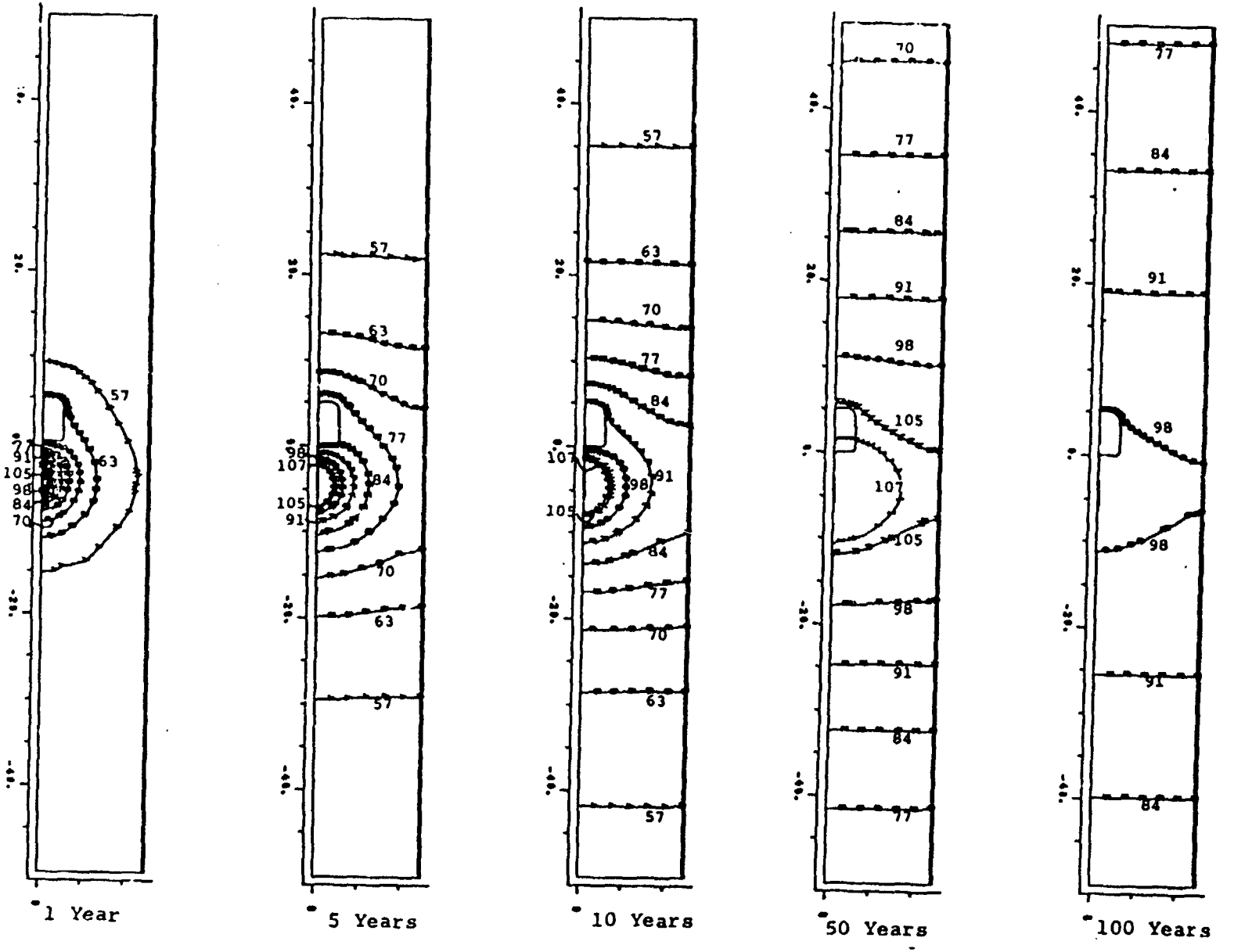

Figure 6. Isotherms at Various Times for HLW
GTL = 75 kw/A, no Boiling of Groundwater

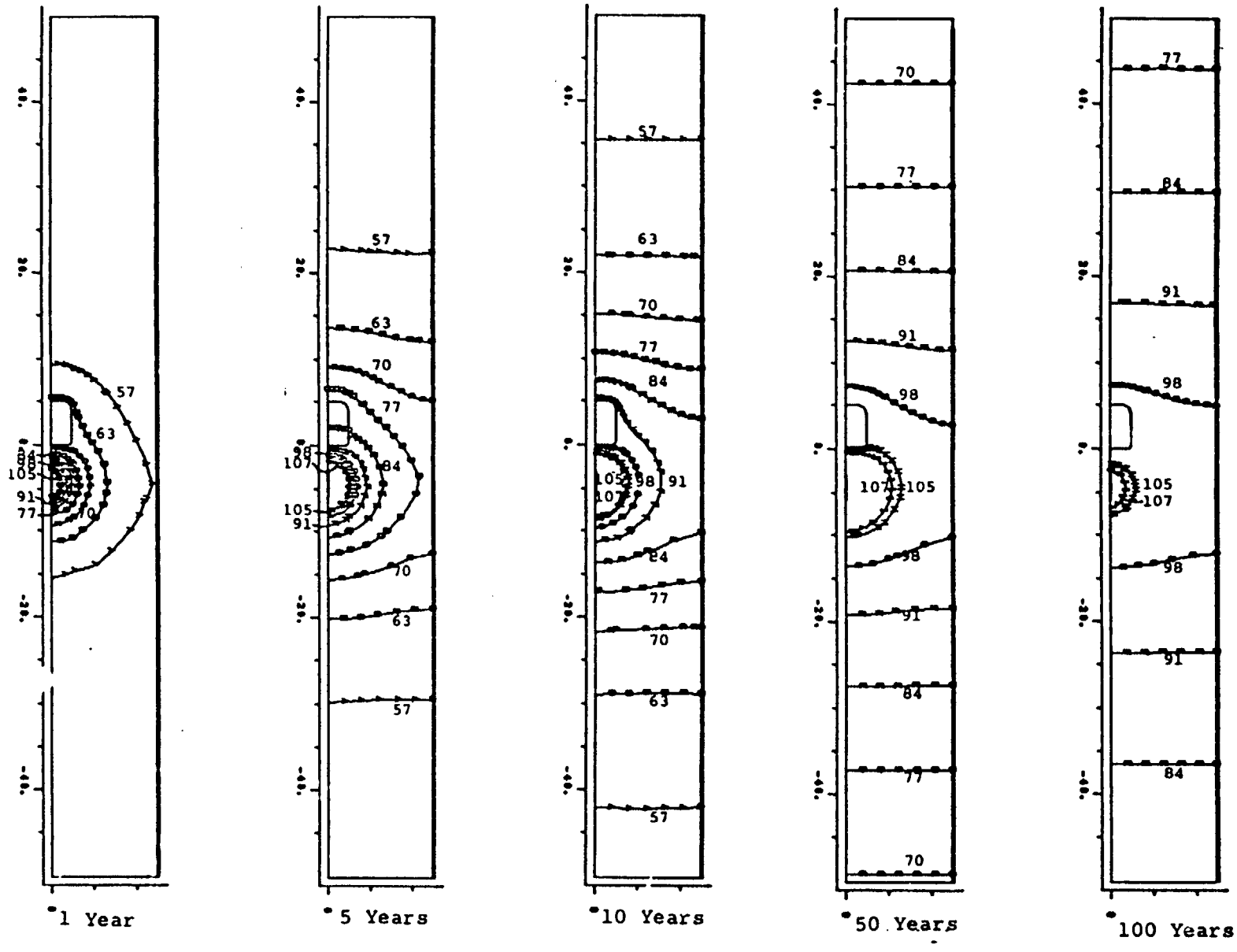

Figure 7. Isotherms at Various Times for HLW
GTL = 100 kw/A, 100°C Boiling of Groundwater

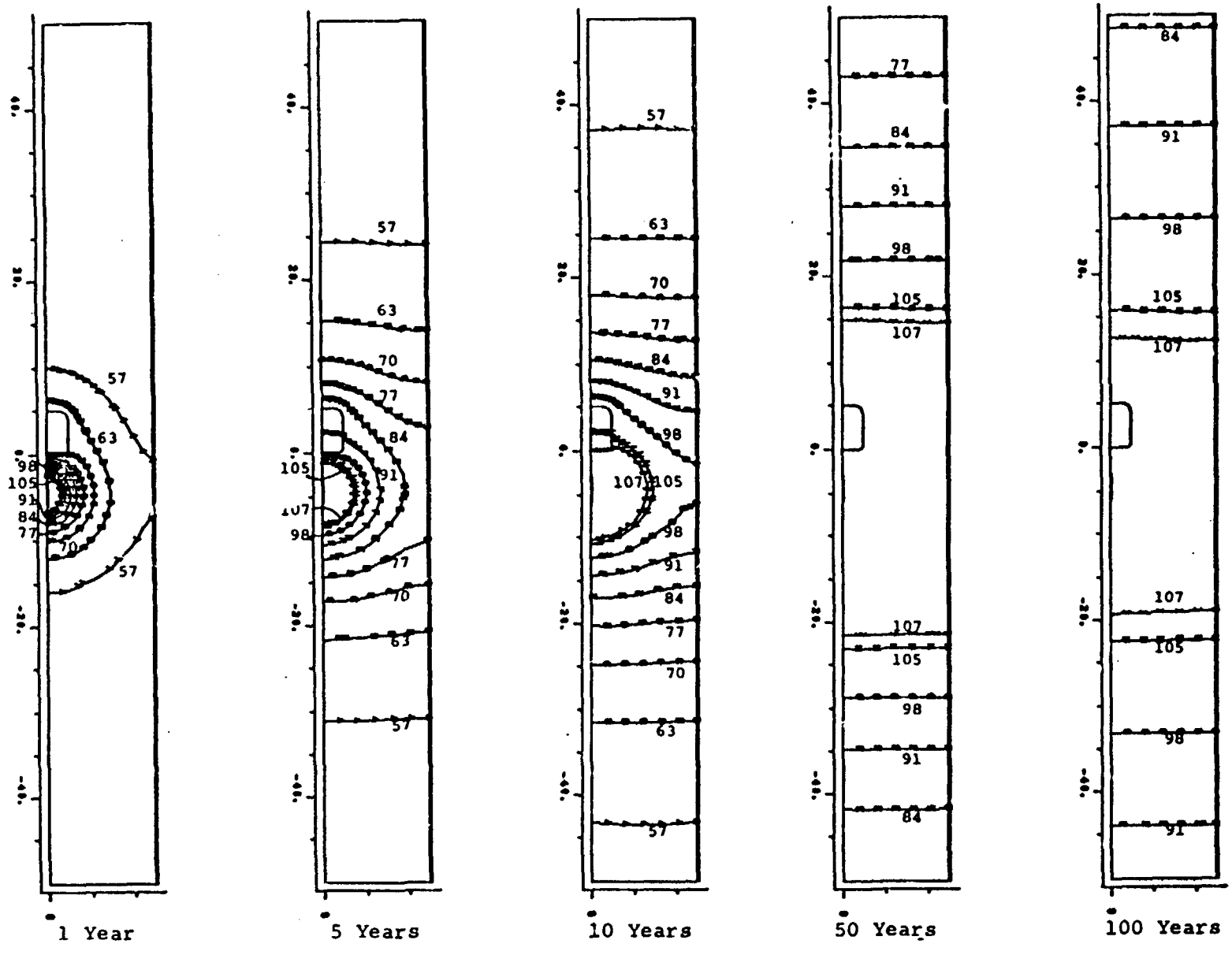

Figure 8. Isotherms at Various Times for HLW
GTL = 100 kw/A, no Boiling of Groundwater

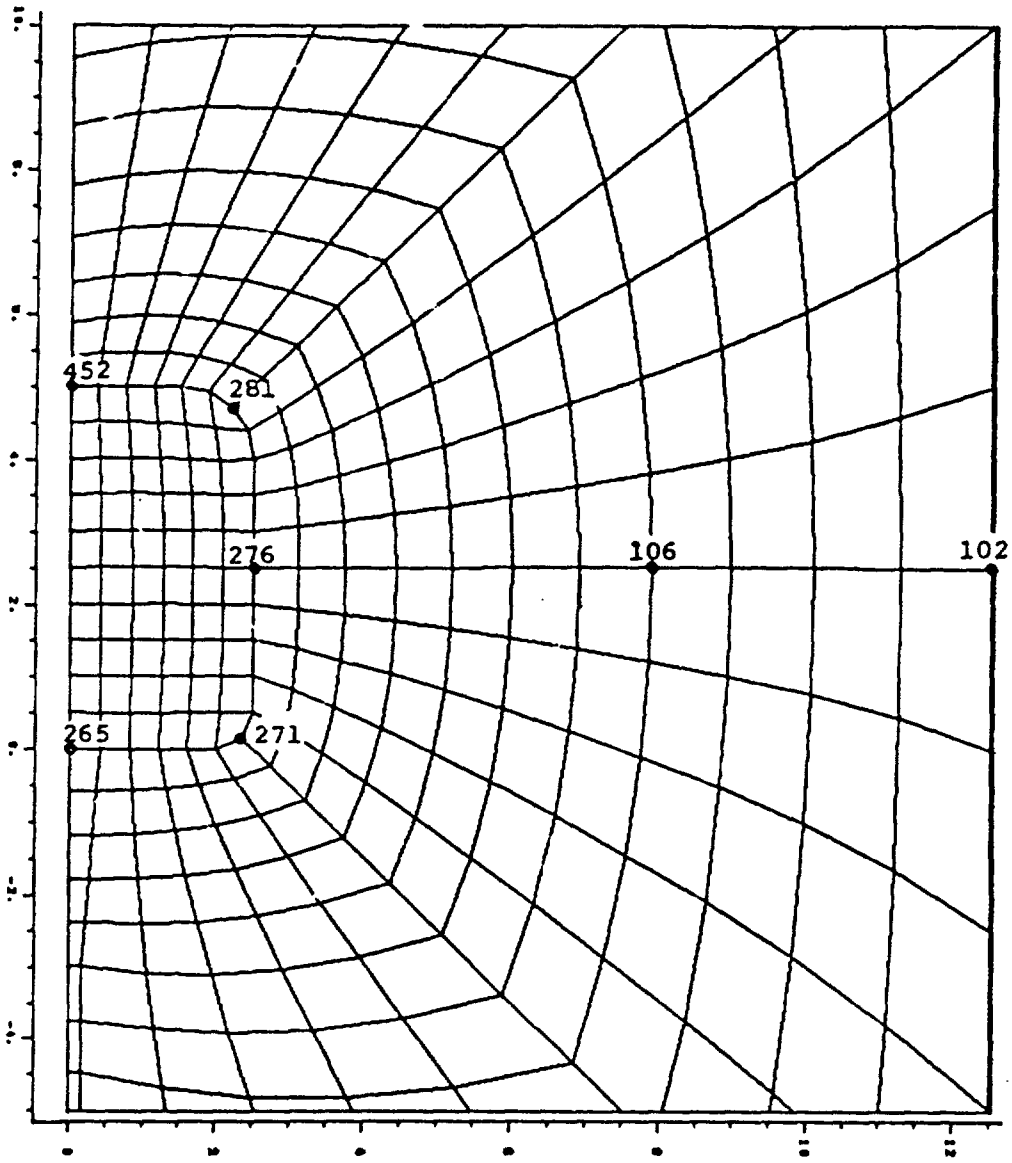

Figure 9. Reference Nodes Used to Identify Locations in the Temperature vs. Time Plots.

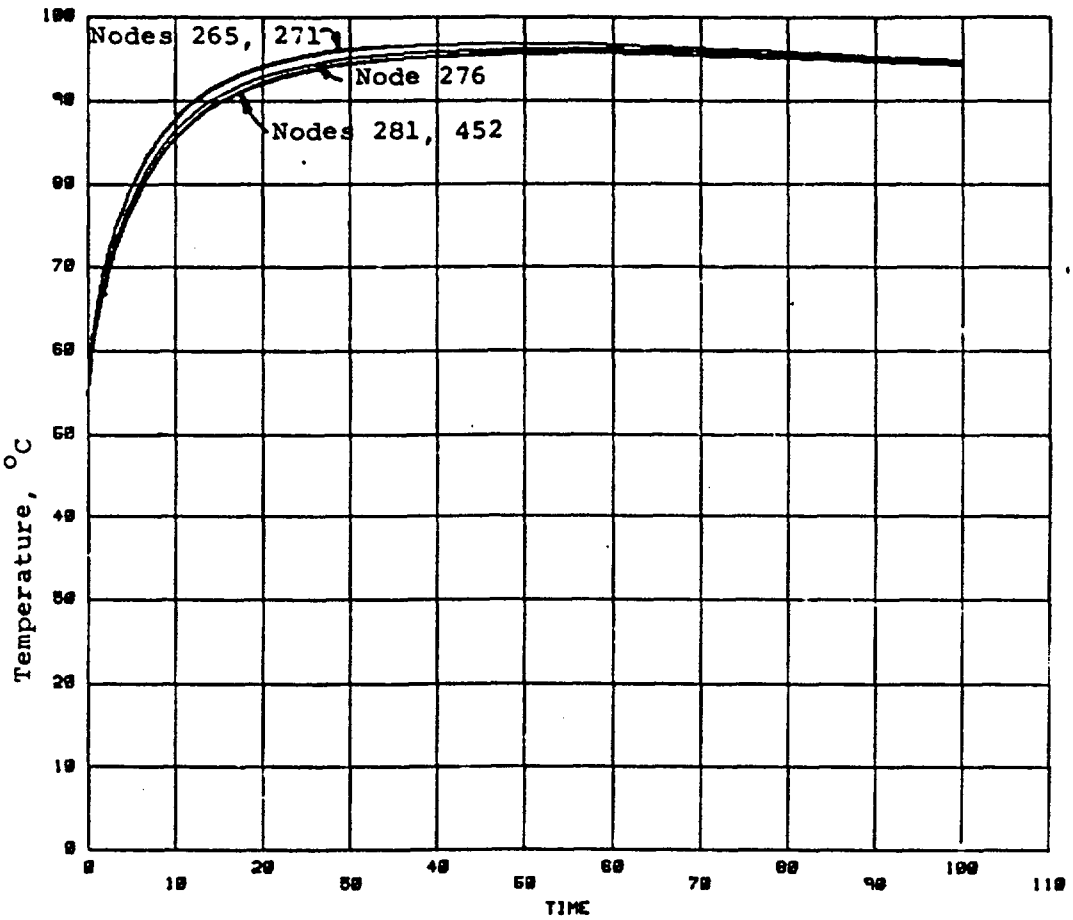

Figure 10. Temperature Histories at Several Locations Around the Room for HLW, GTL = 75 kw/A, Boiling of the Groundwater at 100°C. Time in Years After Emplacement of the Waste.

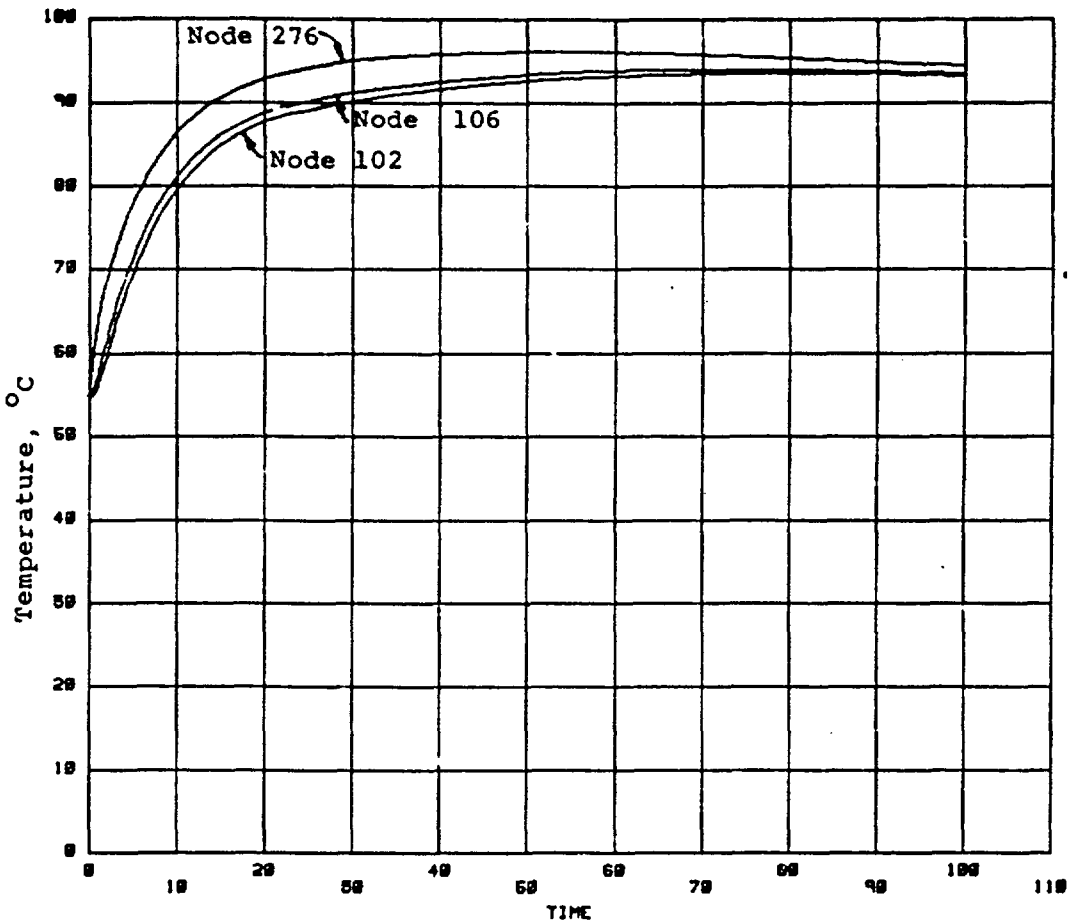

Figure 11. Temperature Histories at Three Locations in the Pillar for HLW, Gtl = 75 kw/A, Boiling of the Groundwater at 100°C. Time in Years After Emplacement of the Waste.

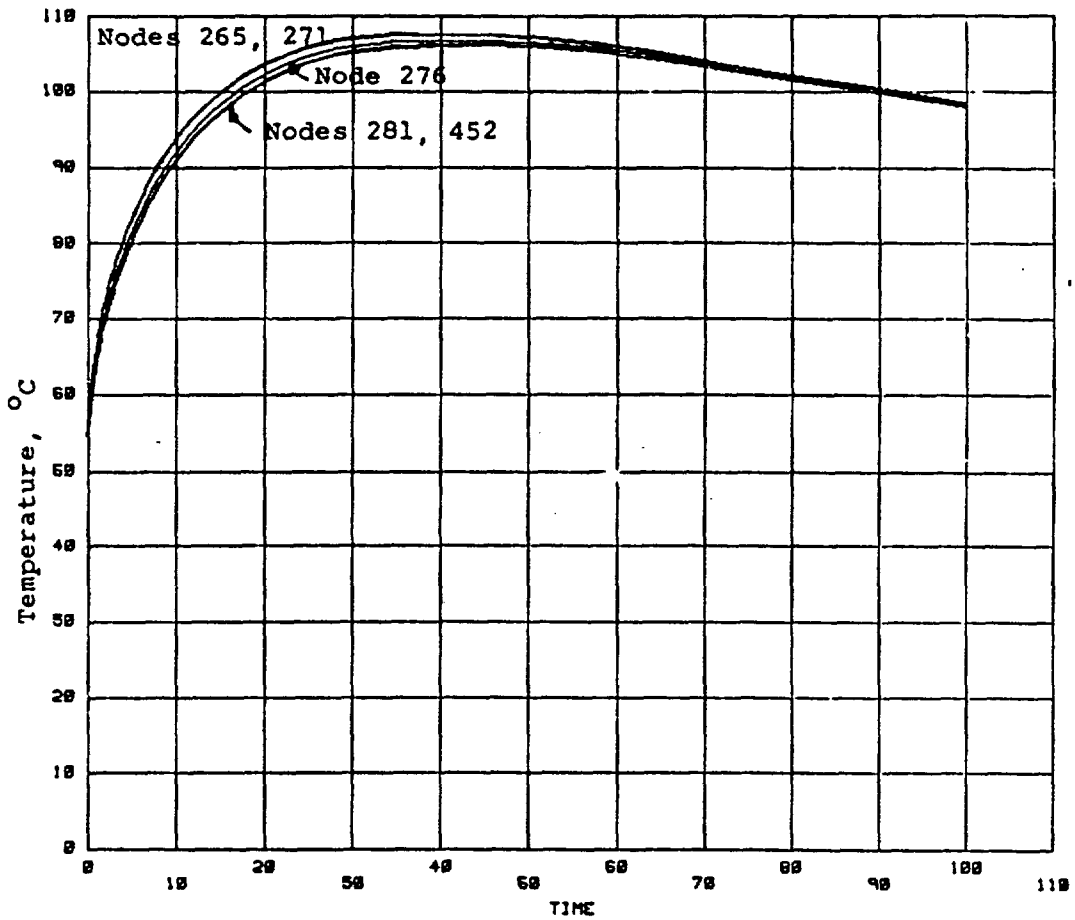

Figure 12. Temperature Histories at Several Locations Around the Room for HLW, GTL = 75 kw/A, no Boiling of the Groundwater. Time in Years After Emplacement of the Waste.

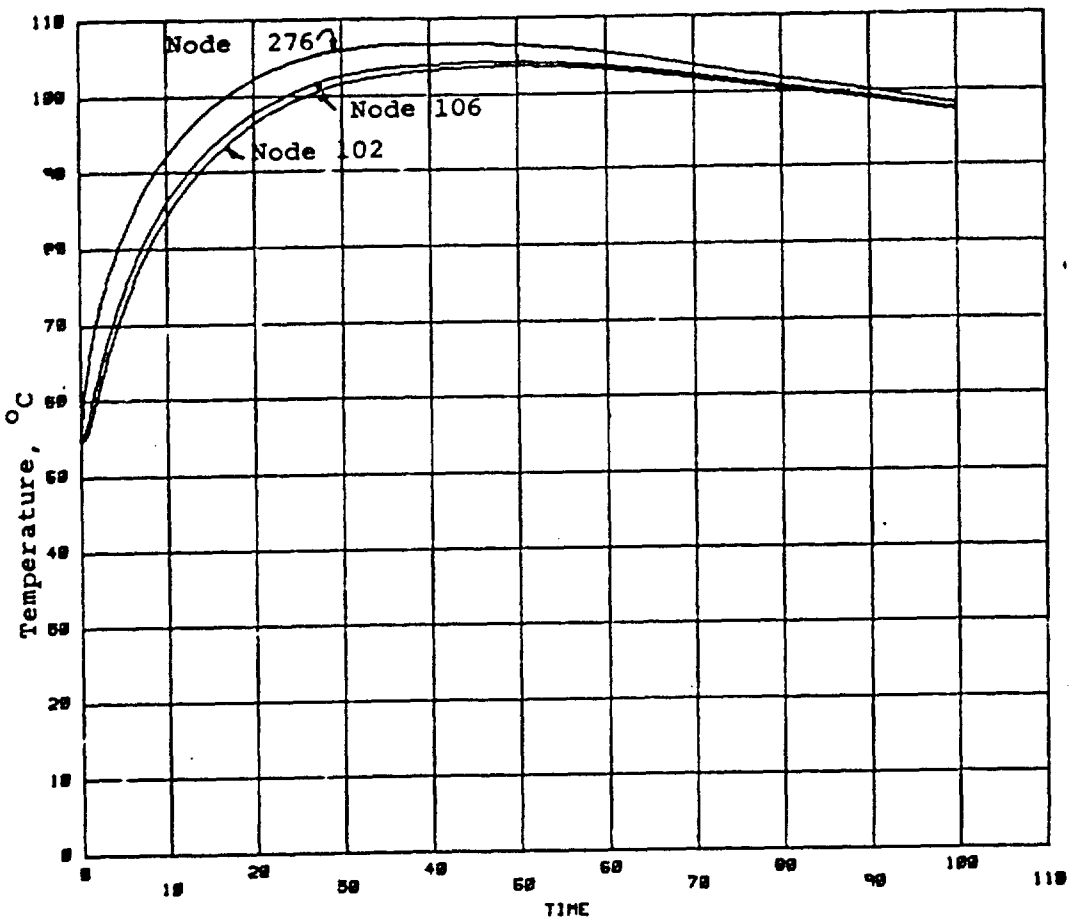

Figure 13. Temperature Histories at Three Locations in the Pillar for HLW, GTL = 75 kw/A, no Boiling of the Groundwater. Time in Years After Emplacement of the Waste.

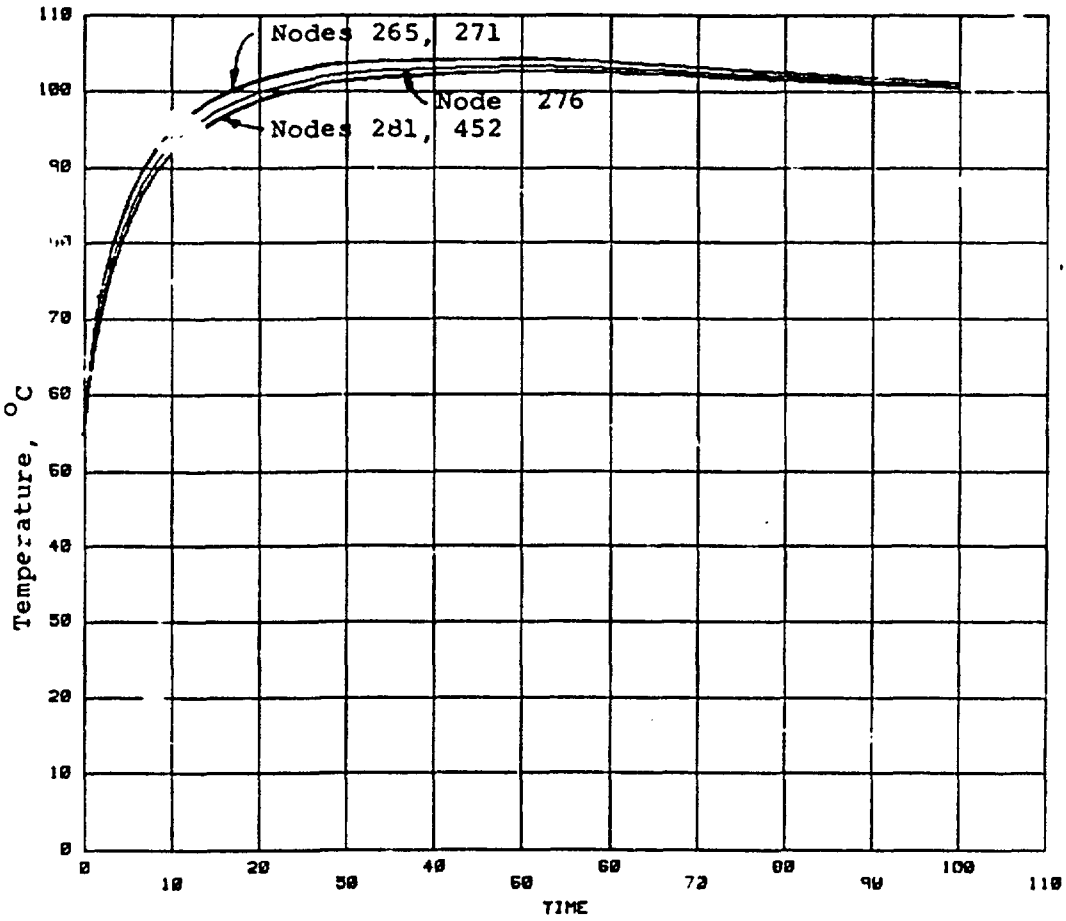

Figure 14. Temperature Histories at Several Locations Around the Room for HLW, GTL = 100 kw/A, Groundwater Boiling at 100°C. Time in Years After Emplacement of the Waste.

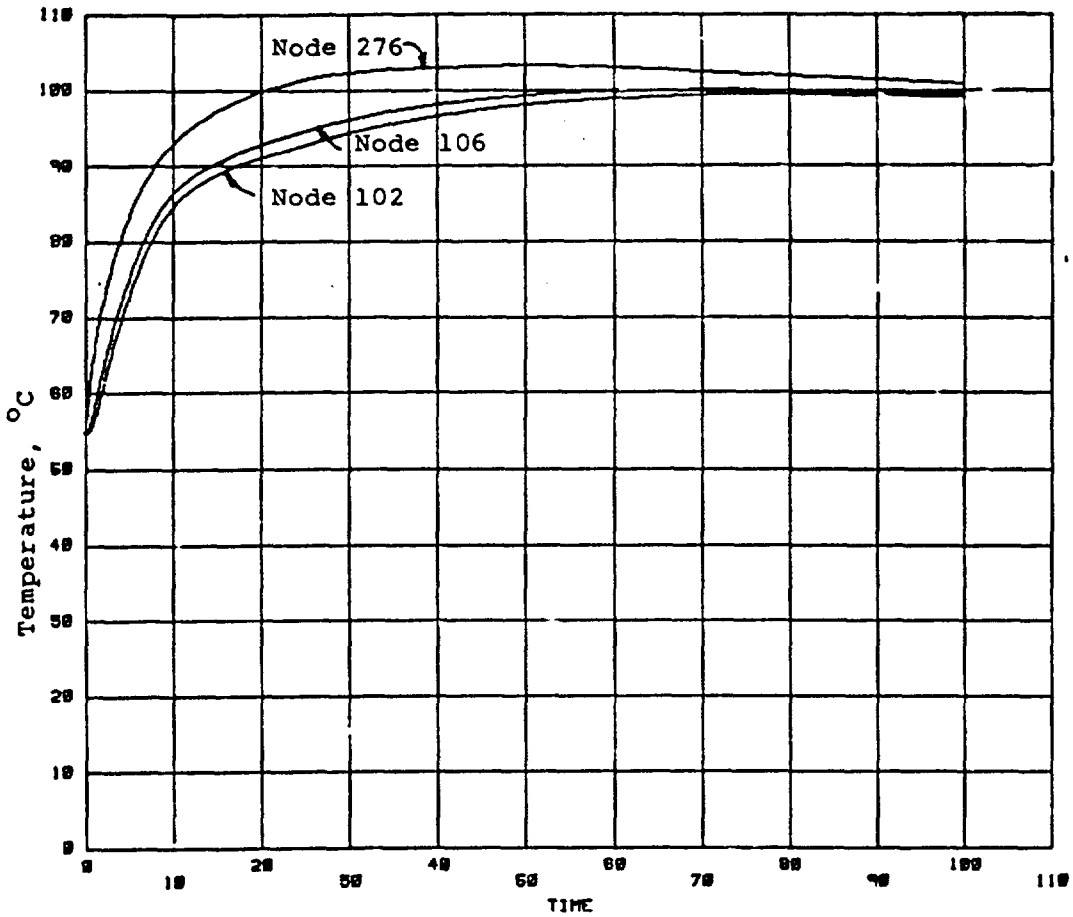

Figure 15. Temperature Histories at Three Locations in the Pillar for HLW, GTL = 100 kw/A, Groundwater Boiling at 100°C. Time in Years After Emplacement of the Waste.

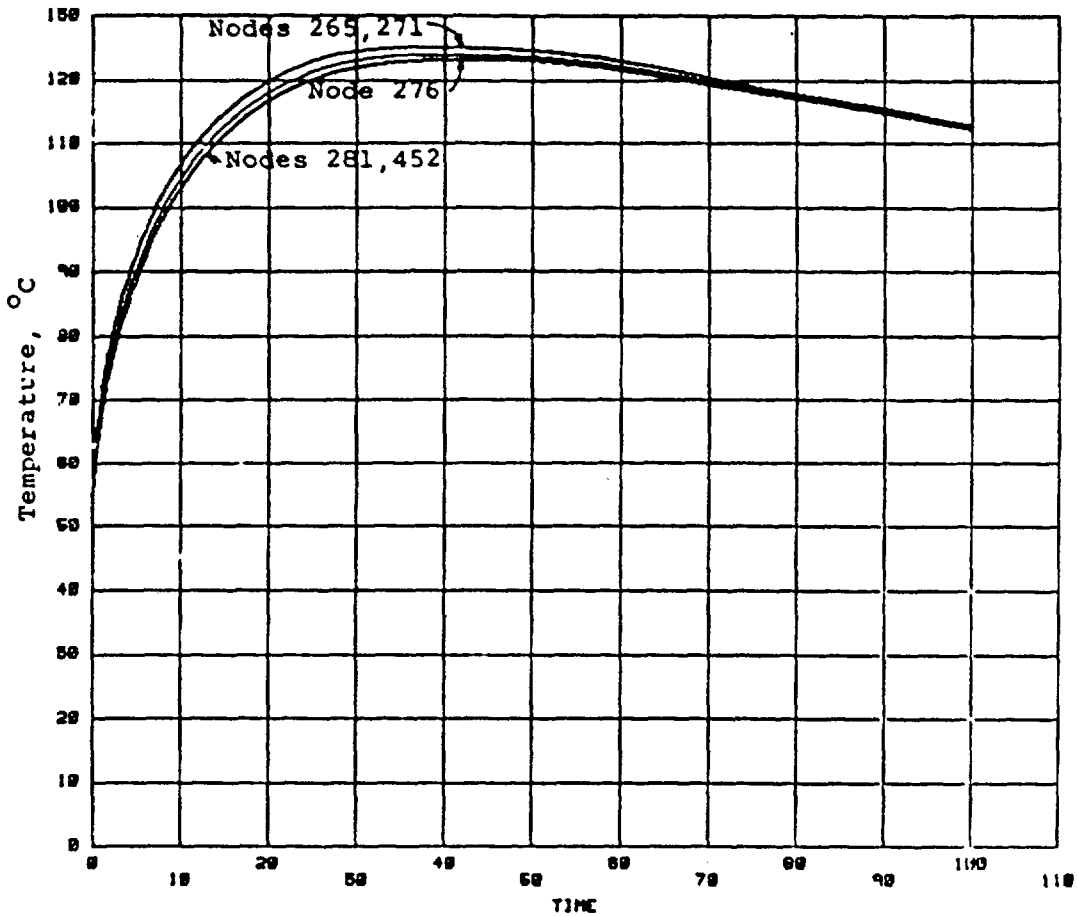

Figure 16. Temperature Histories at Several Locations Around the Room for HLW, GTL = 100 kw/A, no Boiling of the Groundwater. Time in Years After Emplacement of the Waste.

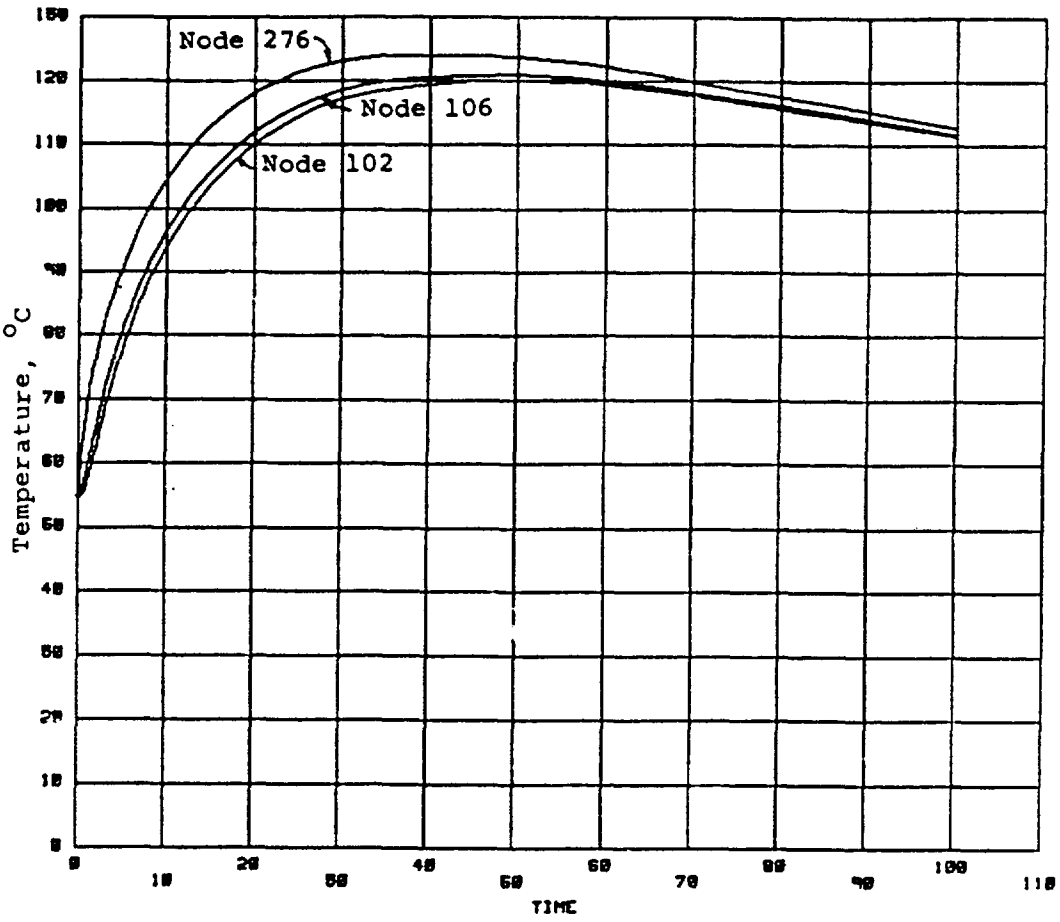

Figure 17. Temperature Histories at Three Locations in the Pillar for HLW, GTL = 100 kw/A, no Boiling of the Groundwater. Time in Years After Emplacement of the Waste.

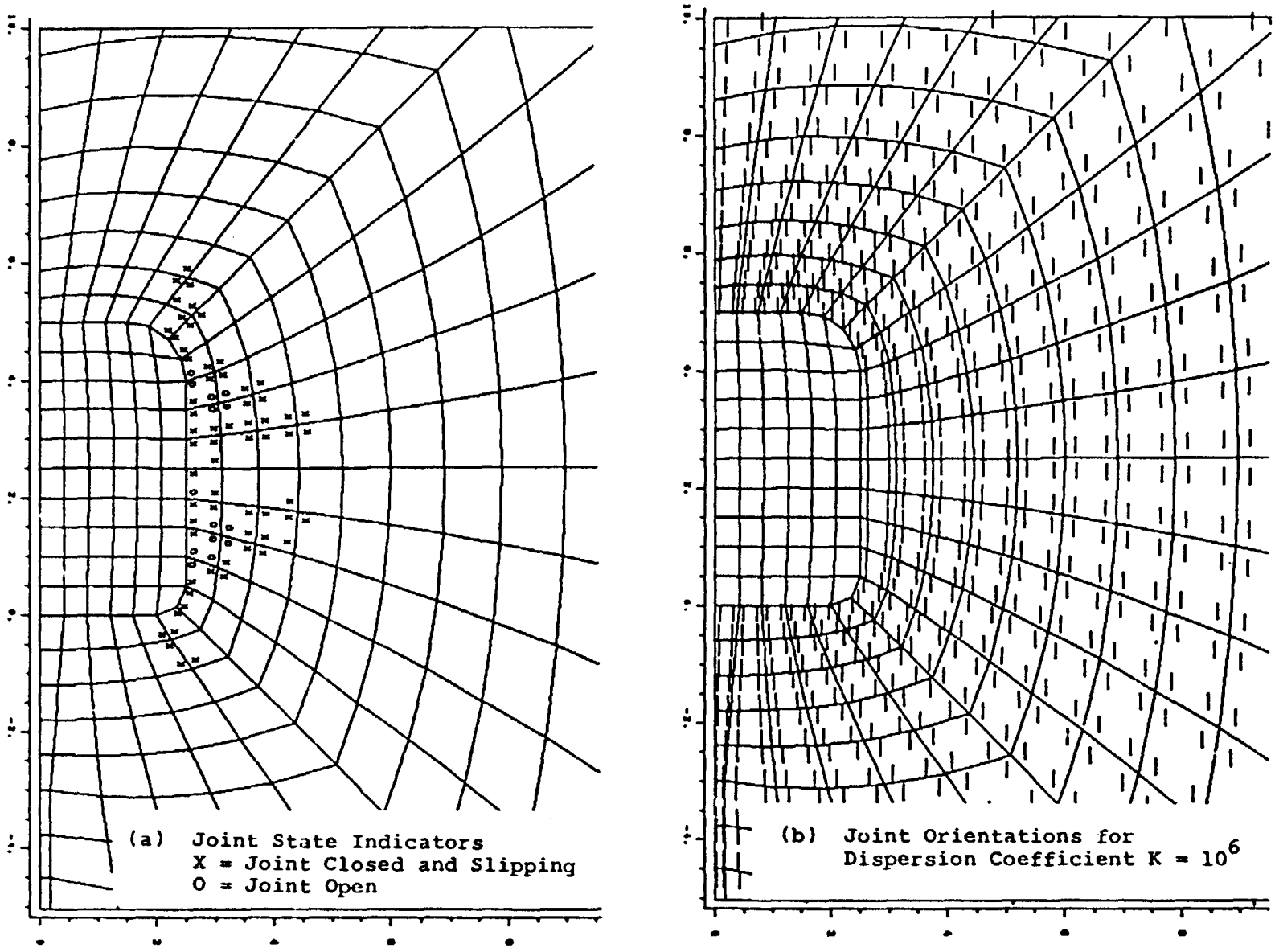

Figure 18. Joint State and Joint Orientations After Excavation of the Room.

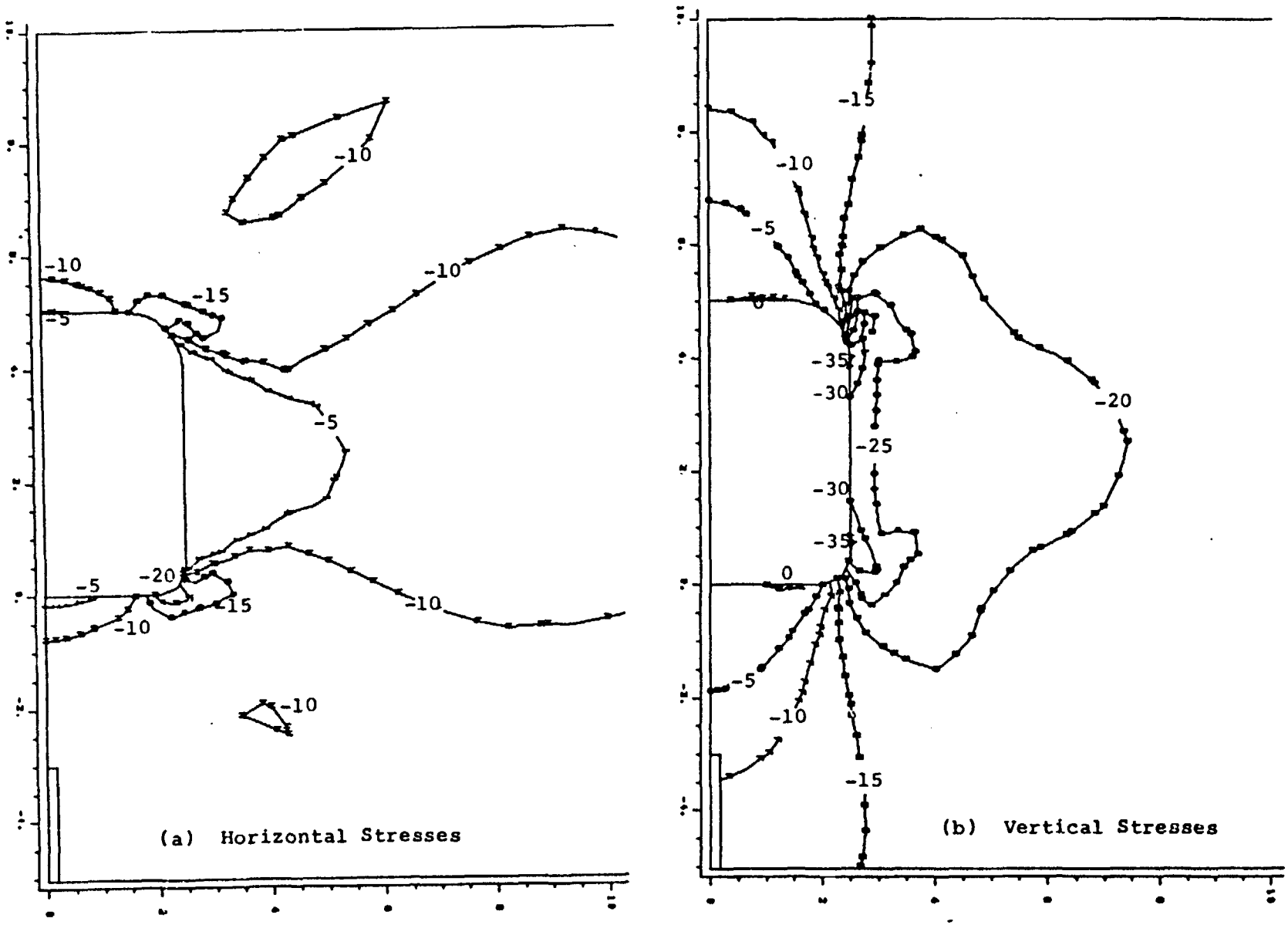

Figure 19. Horizontal and Vertical Stress Contours After Excavation of the Room.

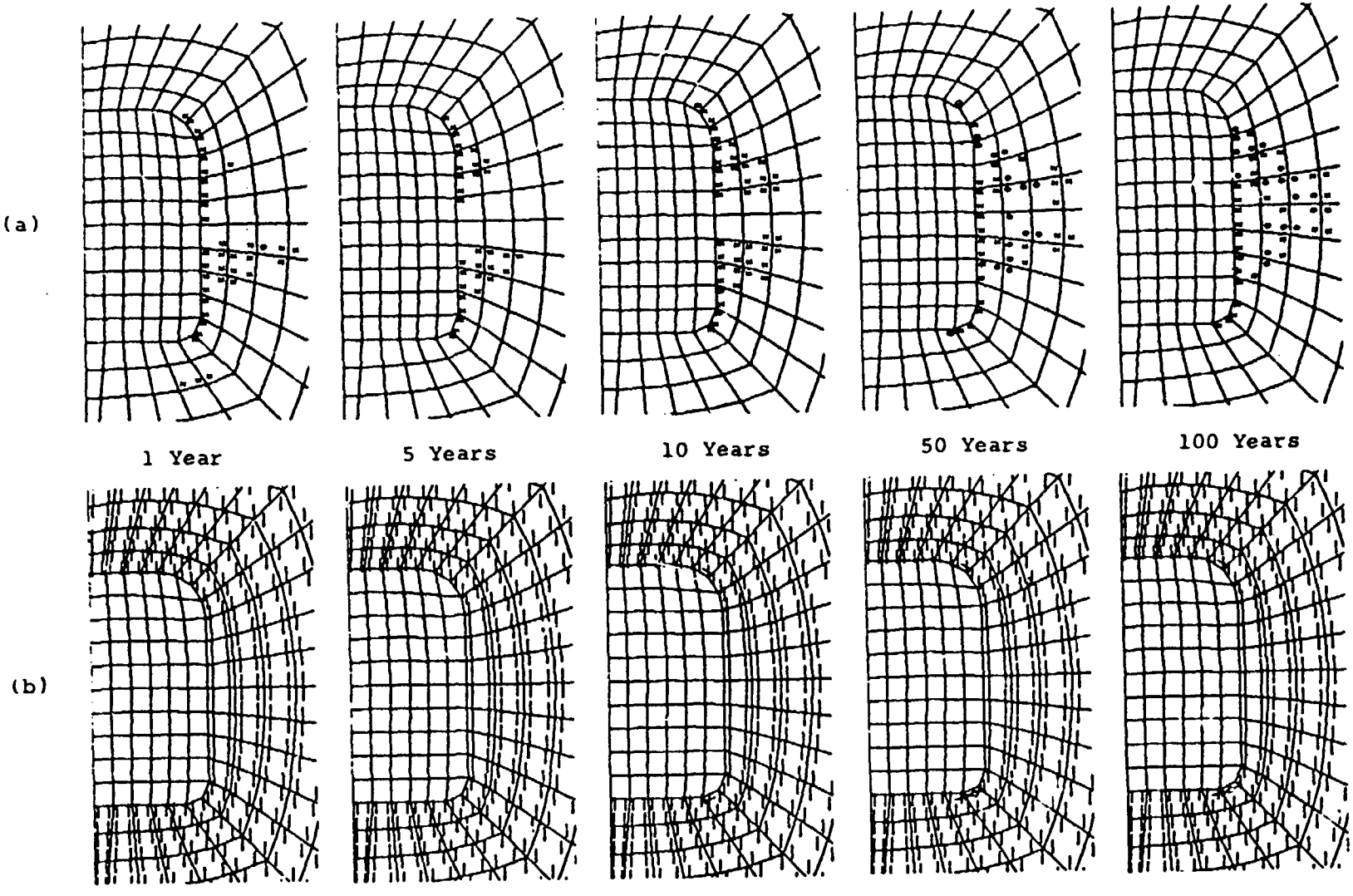

Figure 20. (a) Joint State Indicators at Various Times;
(b) Joint and Crack Orientations at Various Times for HLW, GTL = 75 kw/A, Boiling of the Groundwater at 100°C.

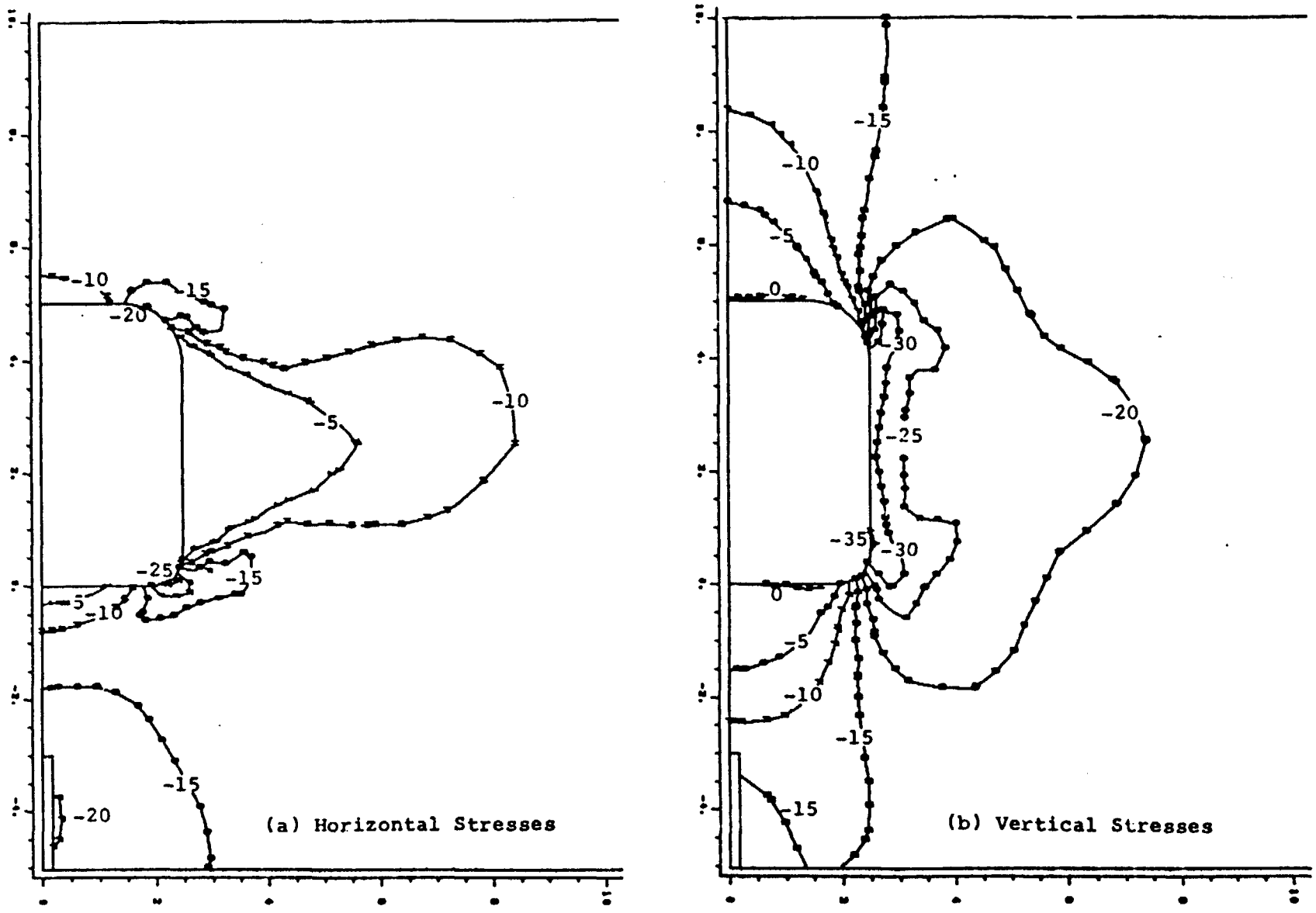

Figure 21. Horizontal and Vertical Stress Contours 1 Year After Emplacement for HLW, GTL = 75 kw/A, Boiling at 100°C.

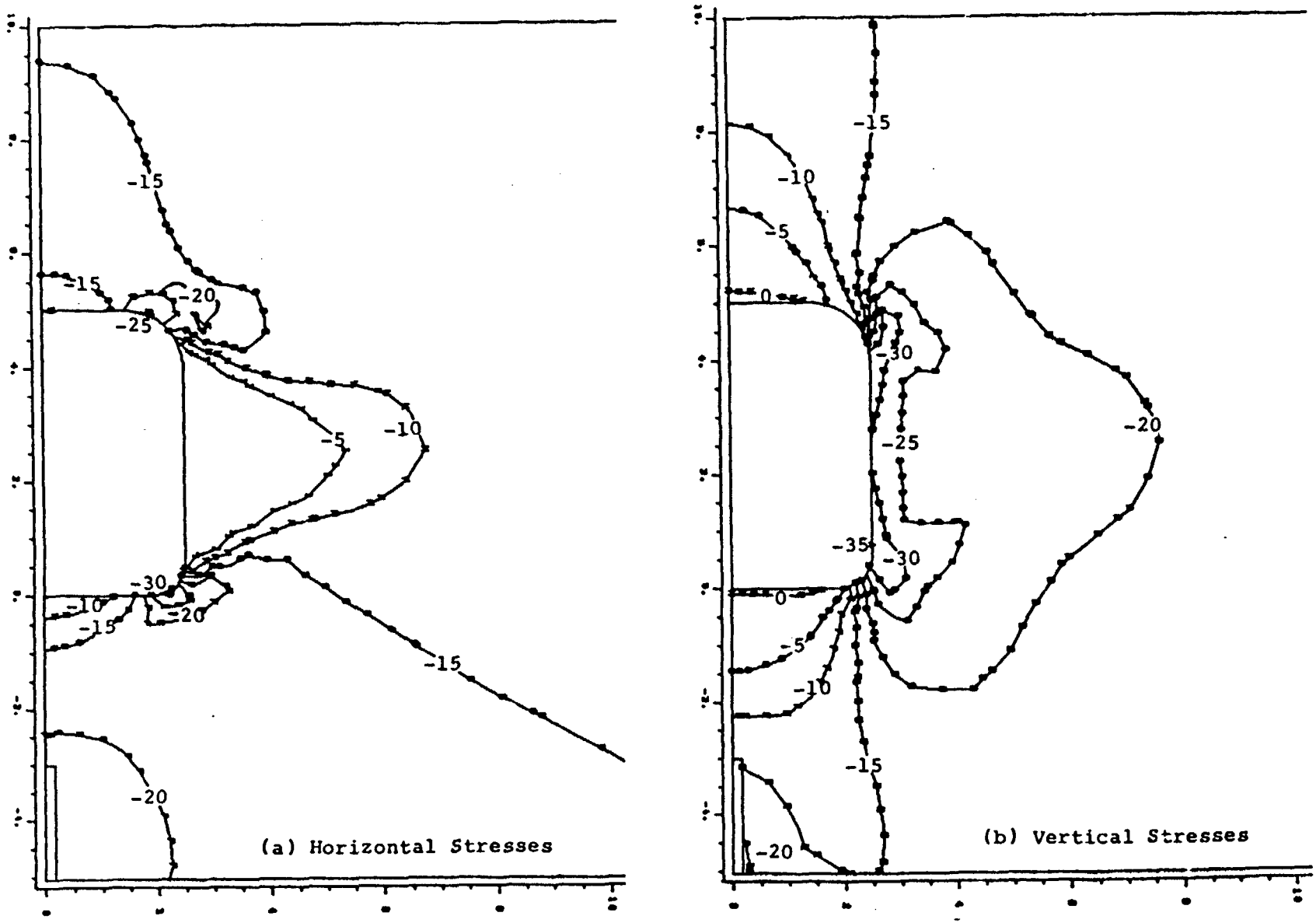

Figure 22. Horizontal and Vertical Stress Contours 5 Years After Emplacement for HLW, GTL = 75 kw/A, Boiling at 100°C.

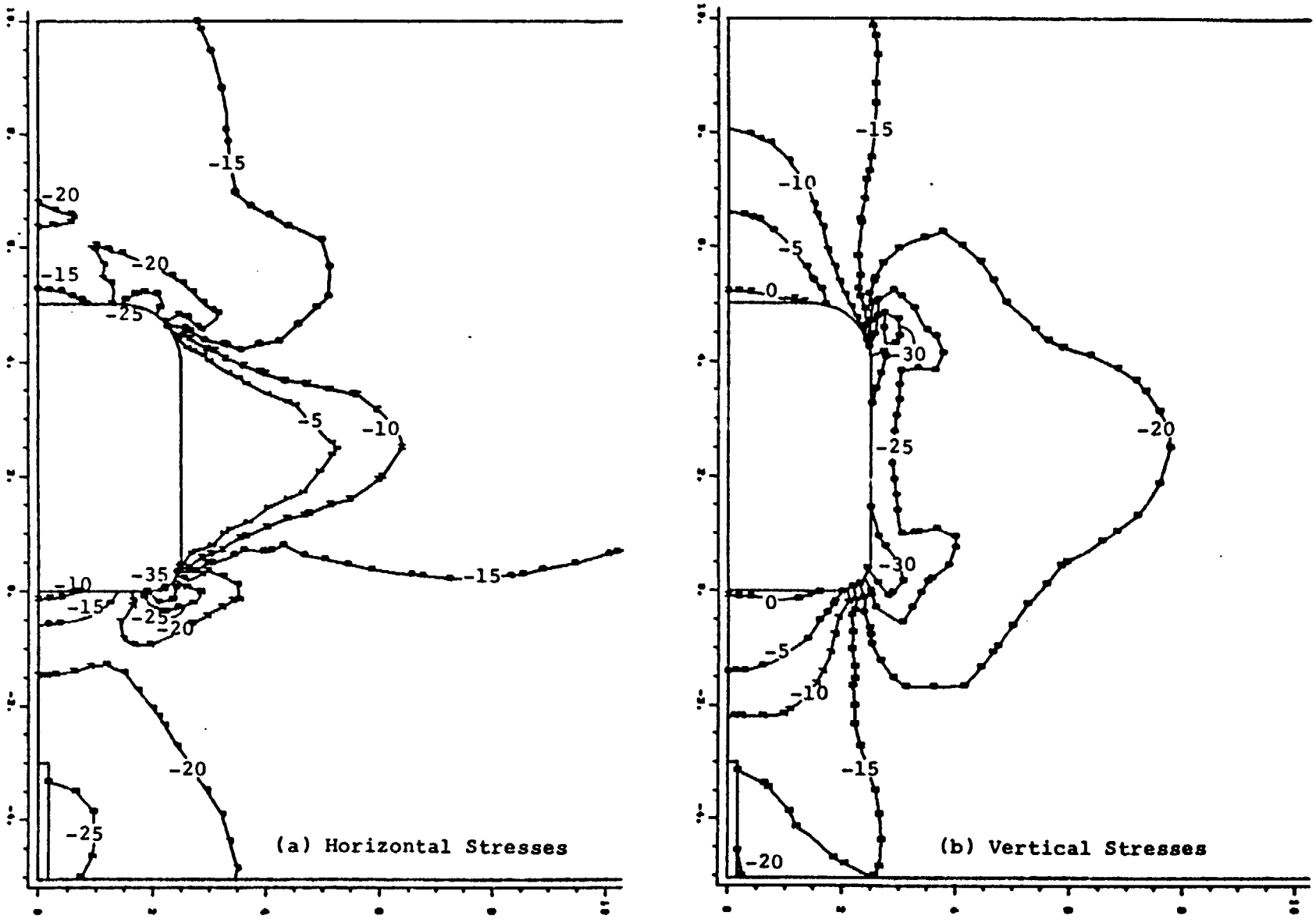

Figure 23. Horizontal and Vertical Stress Contours 10 Years After Emplacement for HLW, GTL = 75 kw/A, Boiling at 100°C.

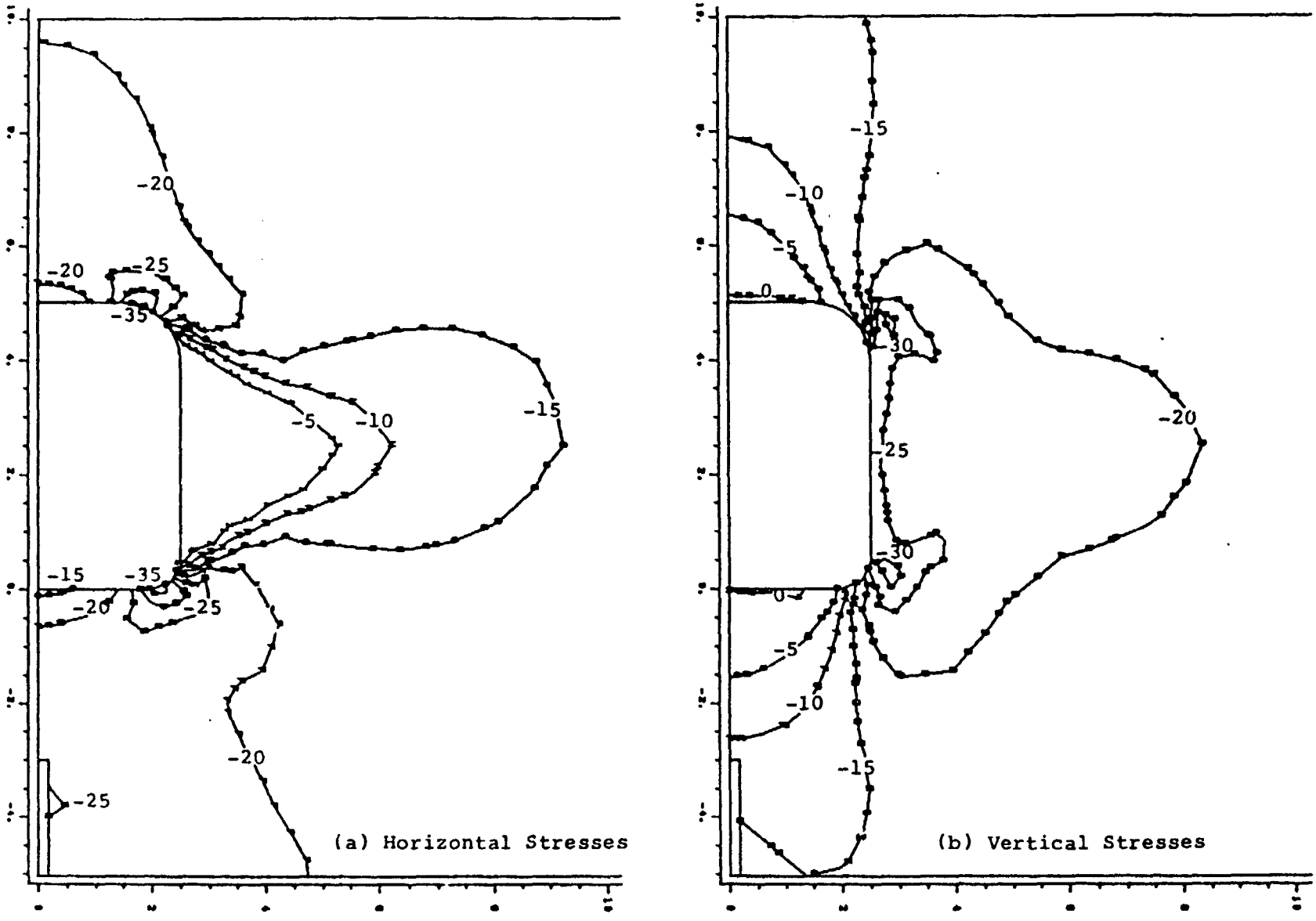

Figure 24. Horizontal and Vertical Stress Contours 50 Years After Emplacement for HLW, GTL = 75 kw/A, Boiling at 100°C.

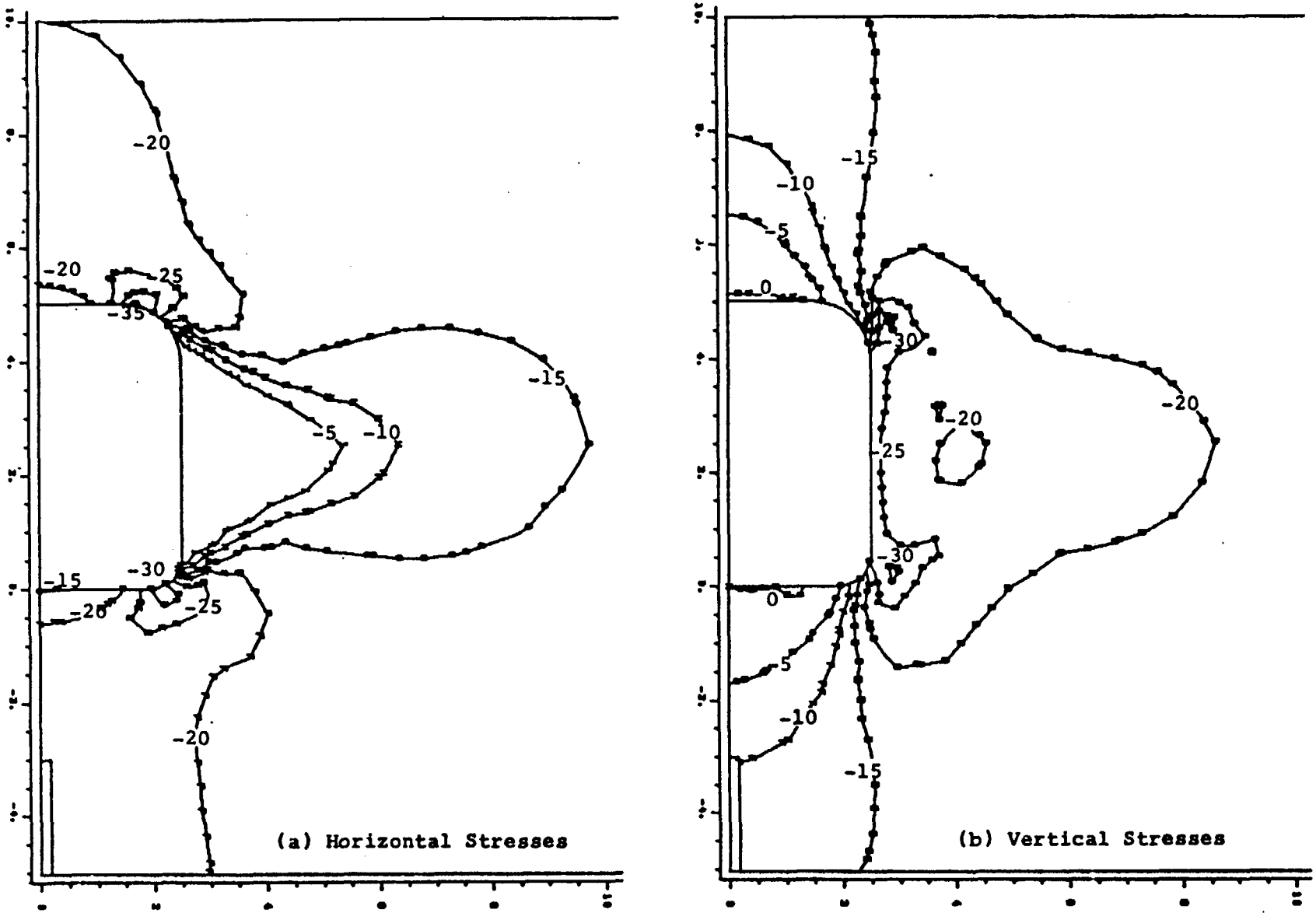

Figure 25. Horizontal and Vertical Stress Contours 100 Years After Emplacement for HLW, GTL = 75 kw/A, Boiling at 100°C.

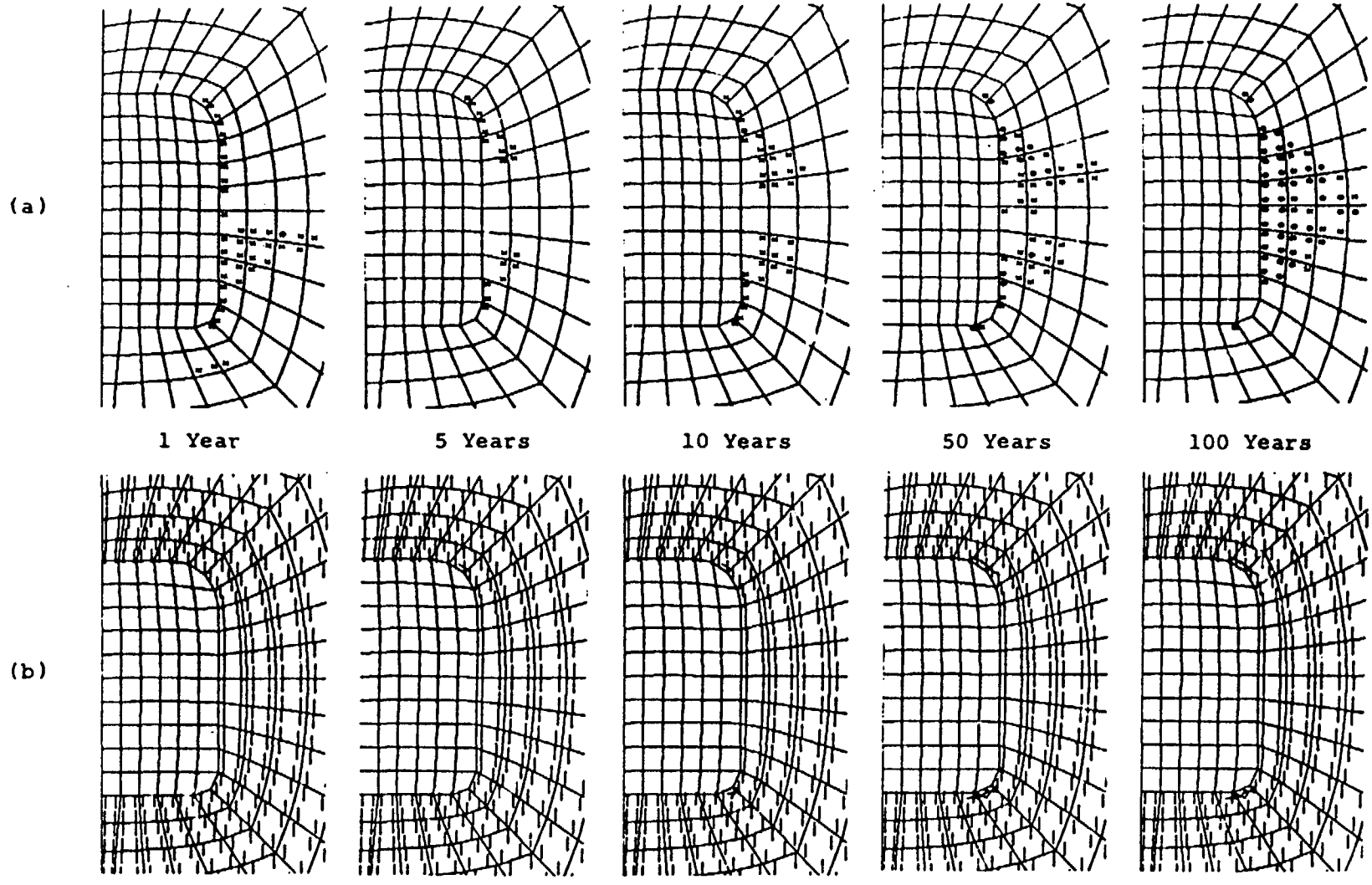

Figure 26. (a) Joint State Indicators at Various Times;
(b) Joint and Crack Orientations at Various Times
for HLW, GTL = 75 kw/A, No Boiling of Groundwater.

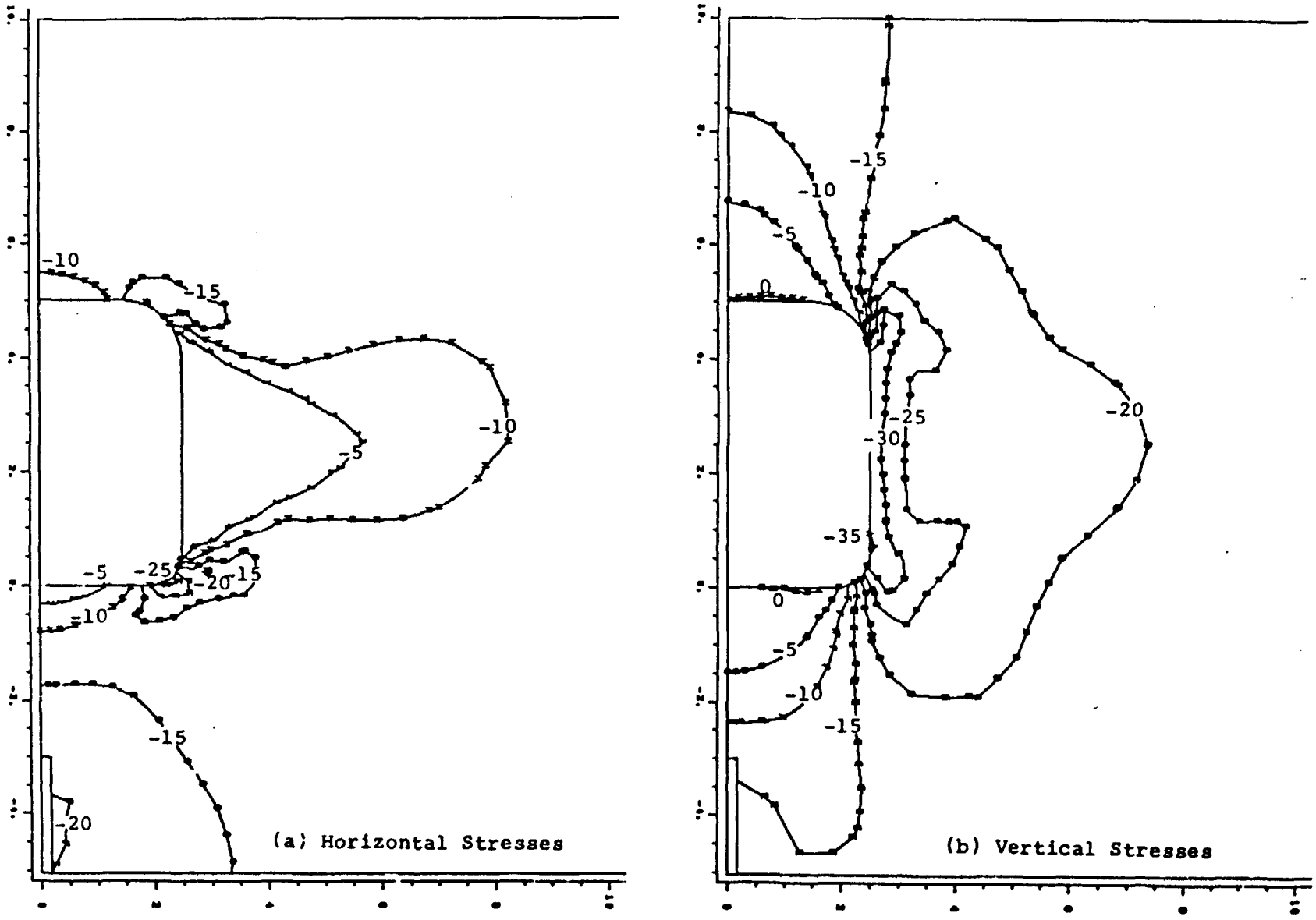

Figure 27. Horizontal and Vertical Stress Contours 1 Year After Emplacement for HLW, GTL = 75 kw/A, No Boiling of Groundwater.

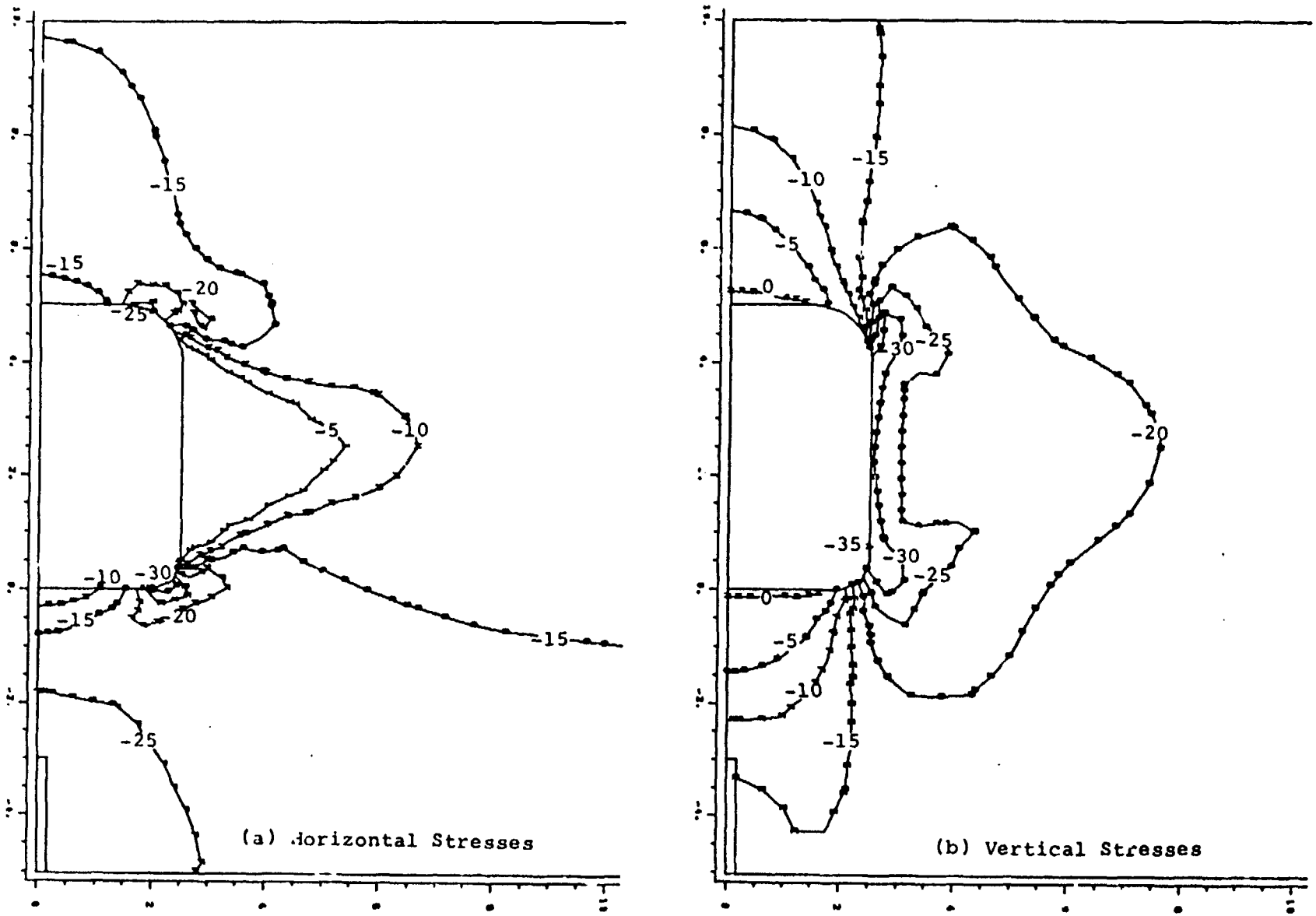

Figure 28. Horizontal and Vertical Stress Contours 5 Years After Emplacement for HLW, GTL = 75 kw/A, No Boiling of Groundwater.

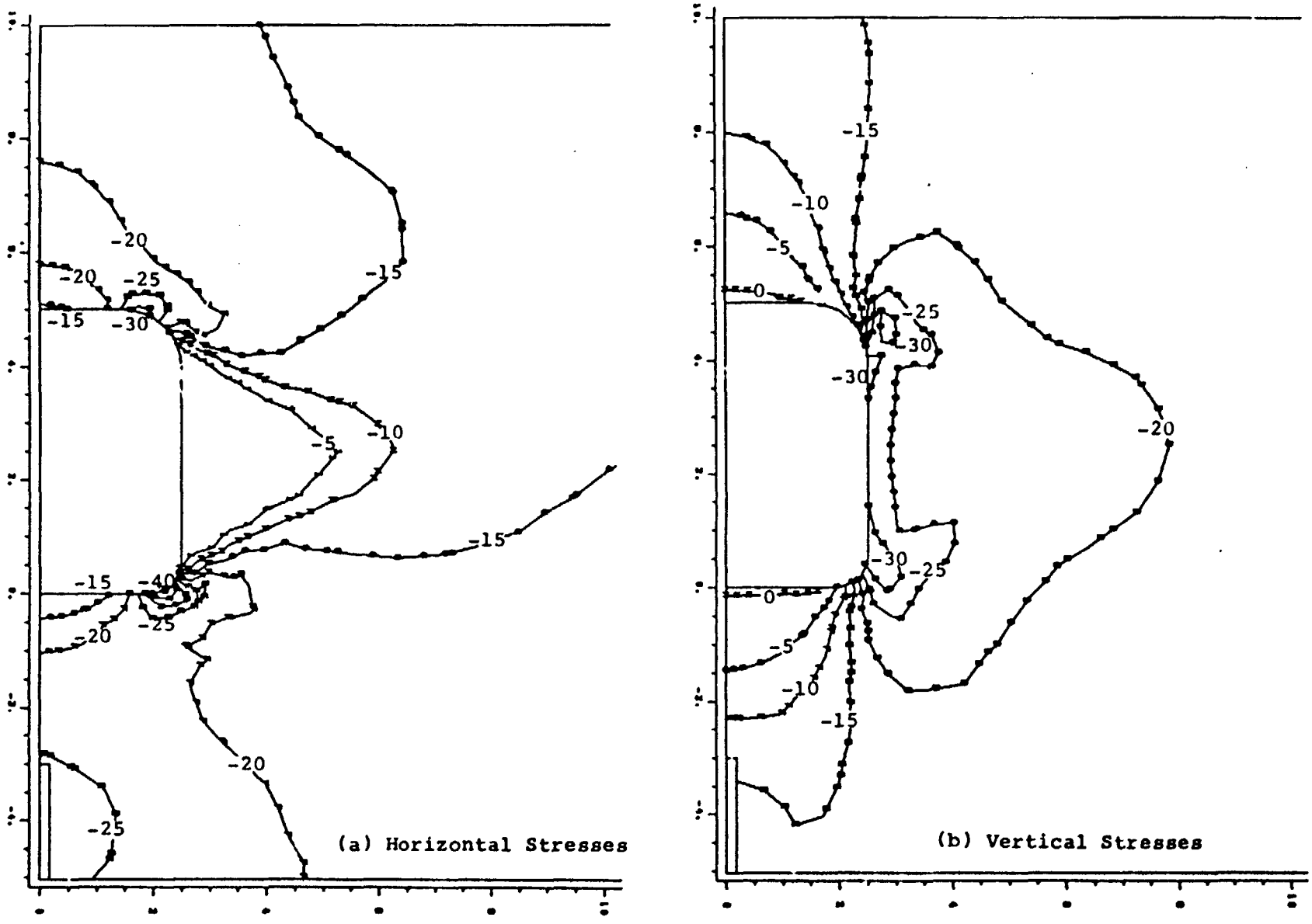

Figure 29. Horizontal and Vertical Stress Contours 10 Years After Emplacement for HLW, GTL = 75 kw/A, No Boiling of Groundwater.

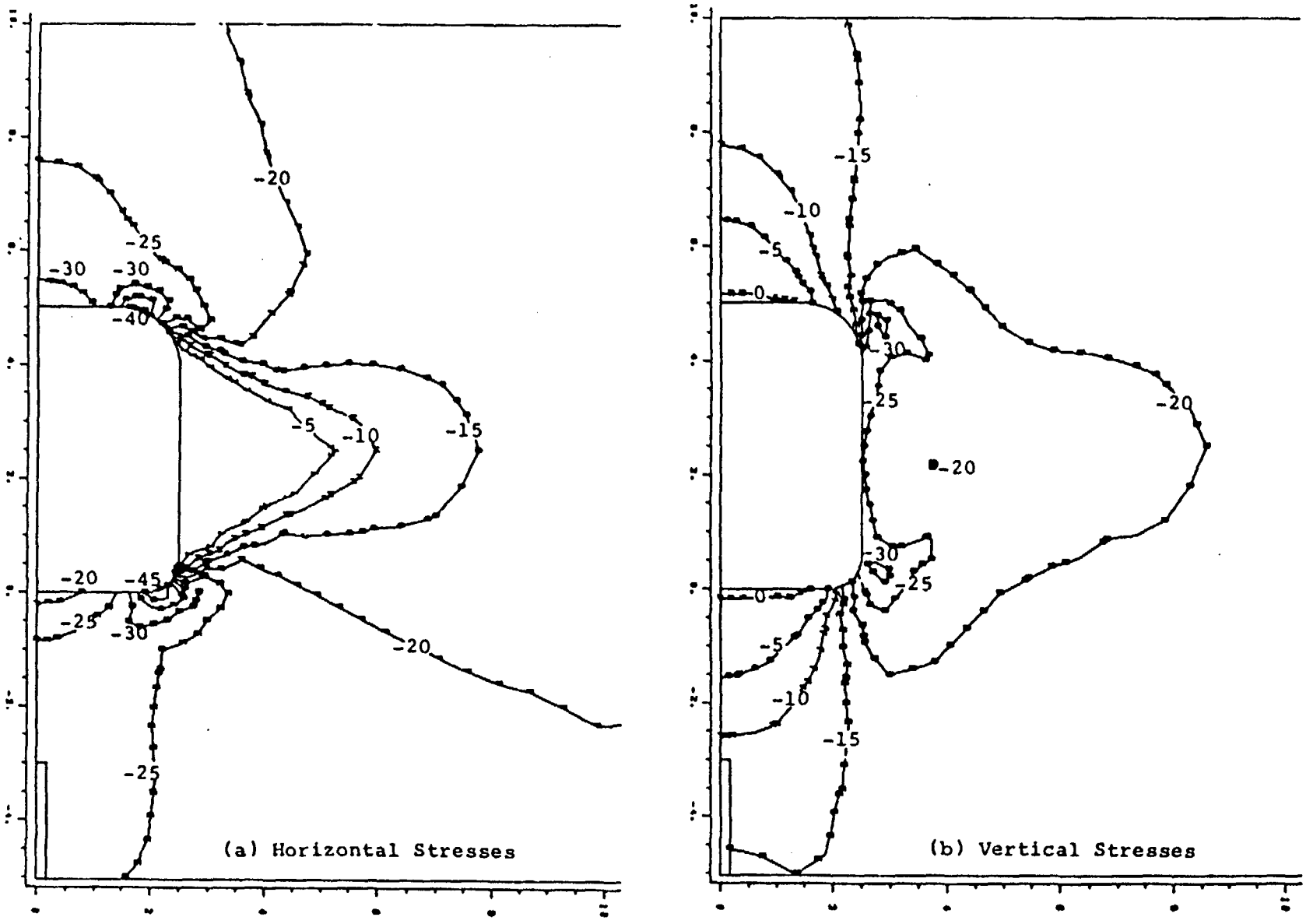

Figure 30. Horizontal and Vertical Stress Contours 50 Years After Emplacement for HLW, GTL = 75 kw/A, No Boiling of Groundwater.

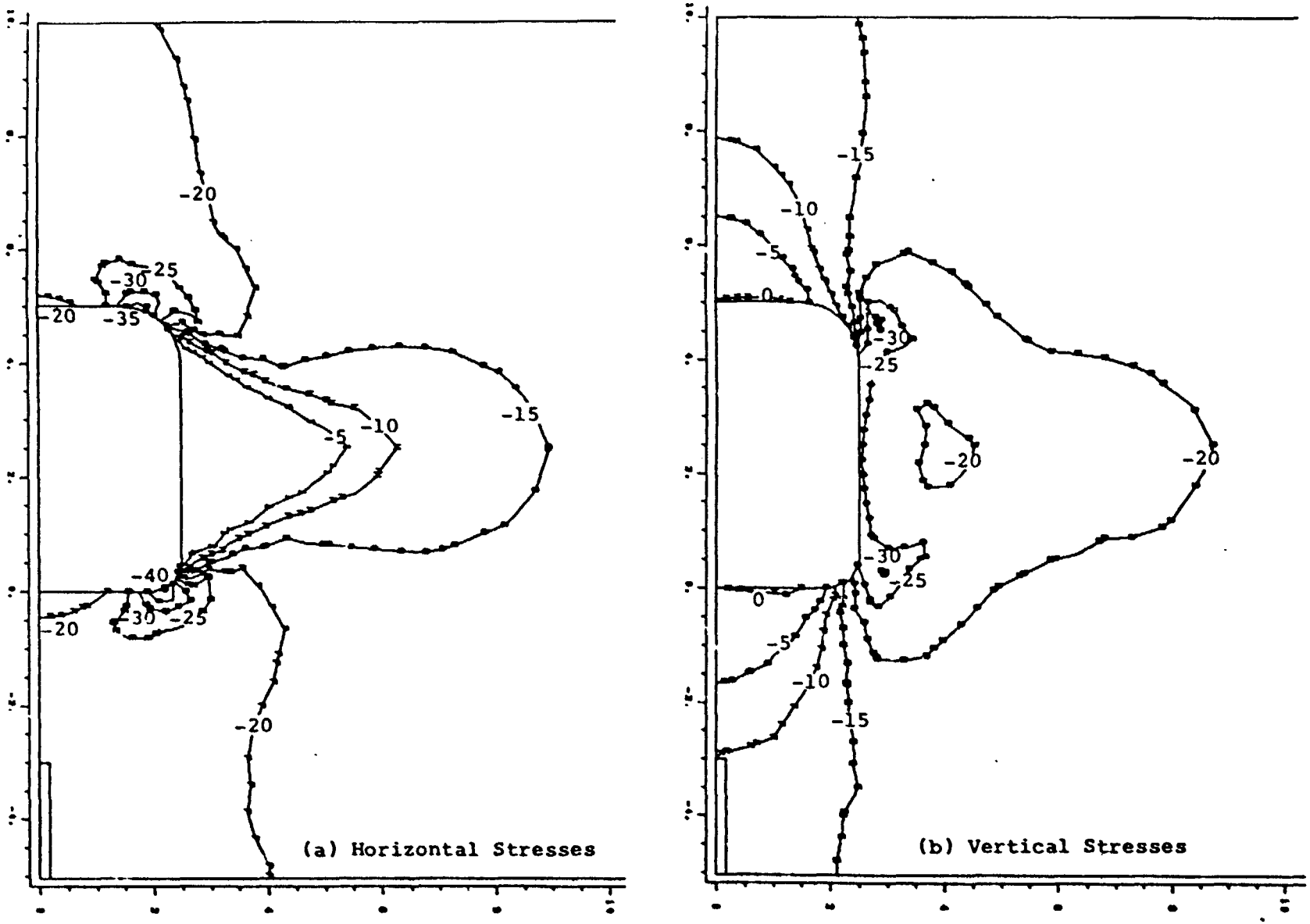

Figure 31. Horizontal and Vertical Stress Contours 100 Years After Emplacement for HLW, GTL = 75 kw/A, No Boiling of Groundwater.

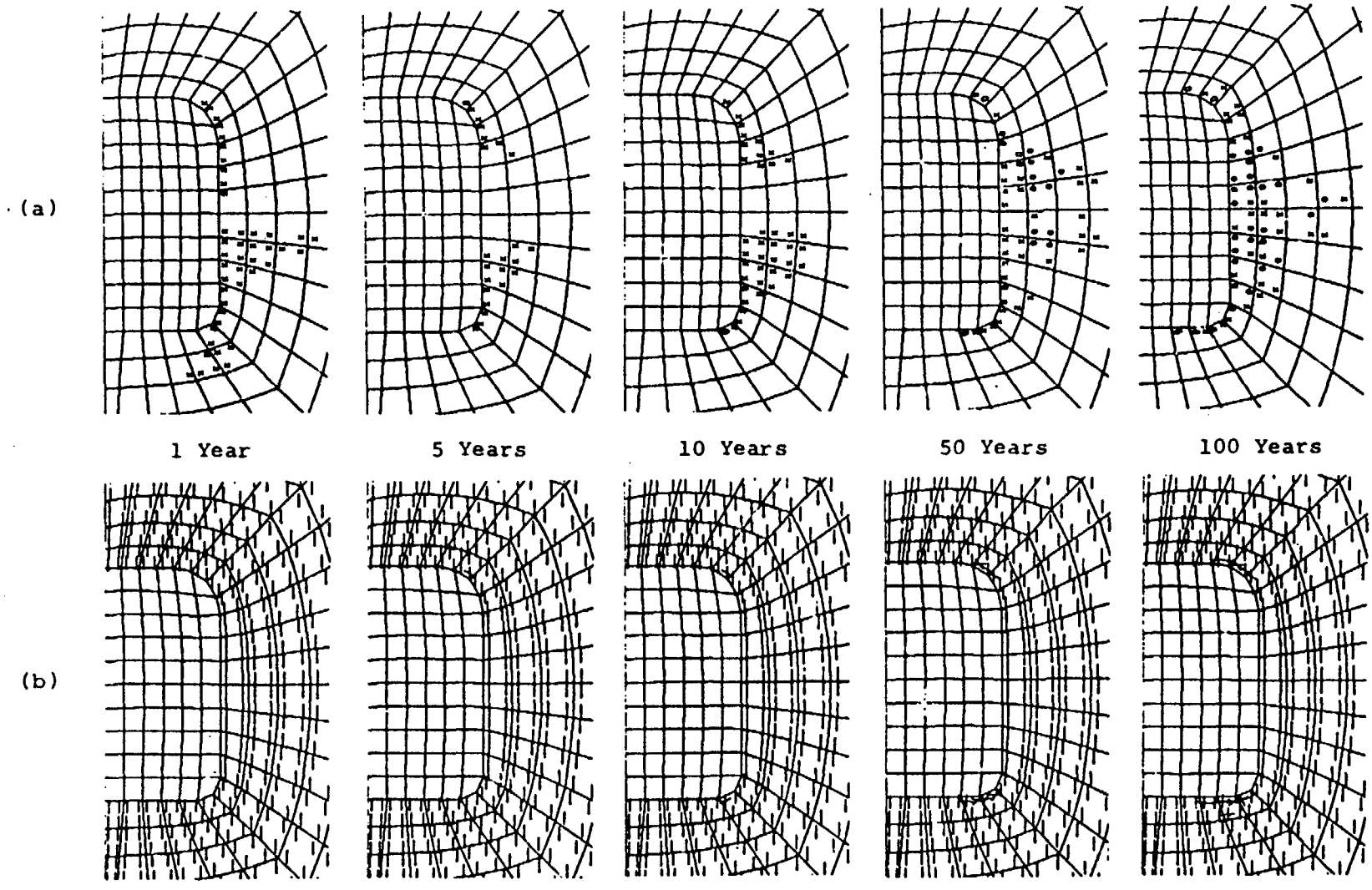

Figure 32. (a) Joint State Indicators at Various Times;
(b) Joint and Crack Orientations at Various Times
for HLW, GTL =100 kw/A, Boiling at 100°C.

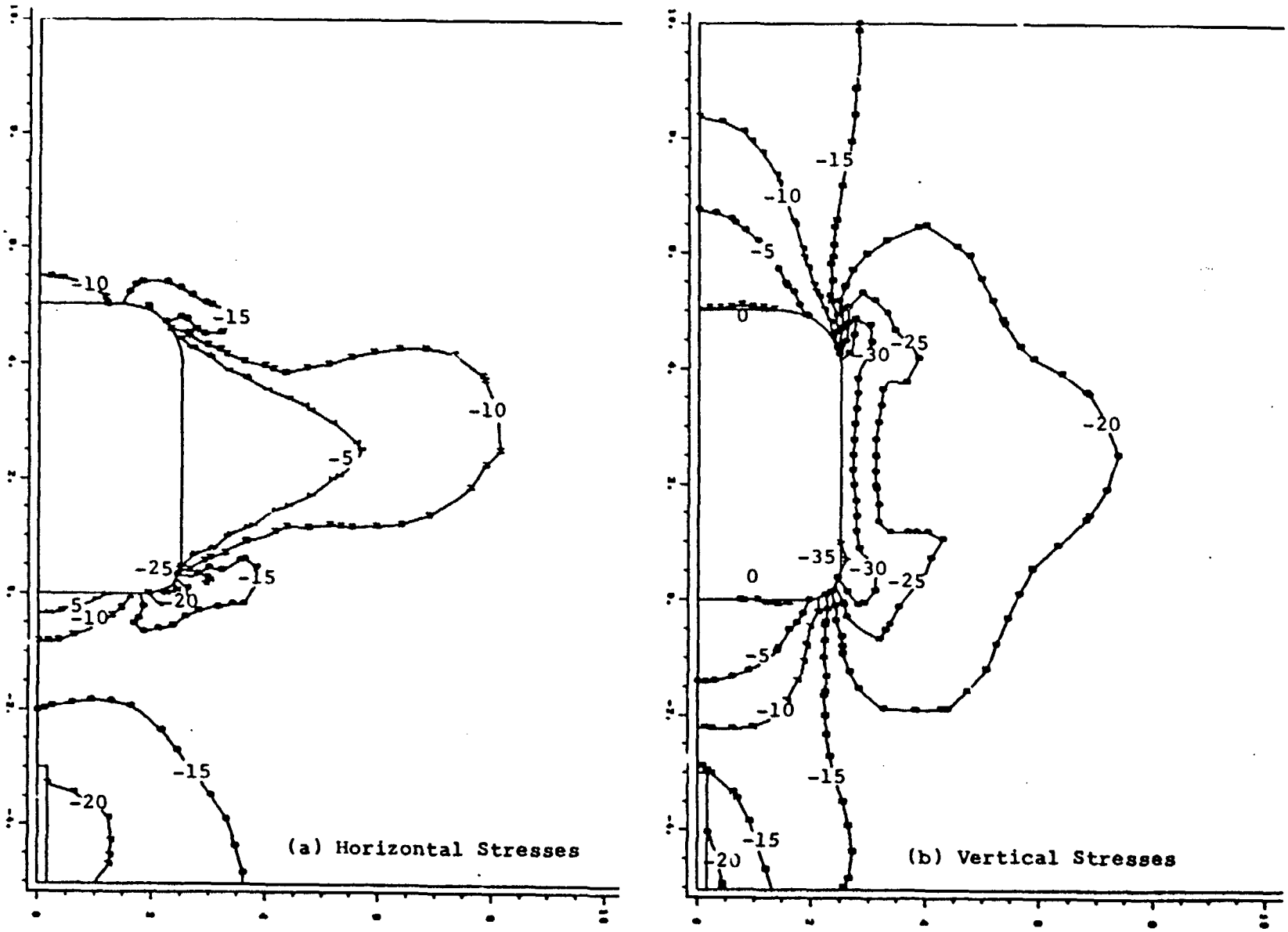

Figure 33. Horizontal and Vertical Stress Contours 1 Year After Emplacement for HLW, GTL = 100 kw/A, Boiling at 100°C.

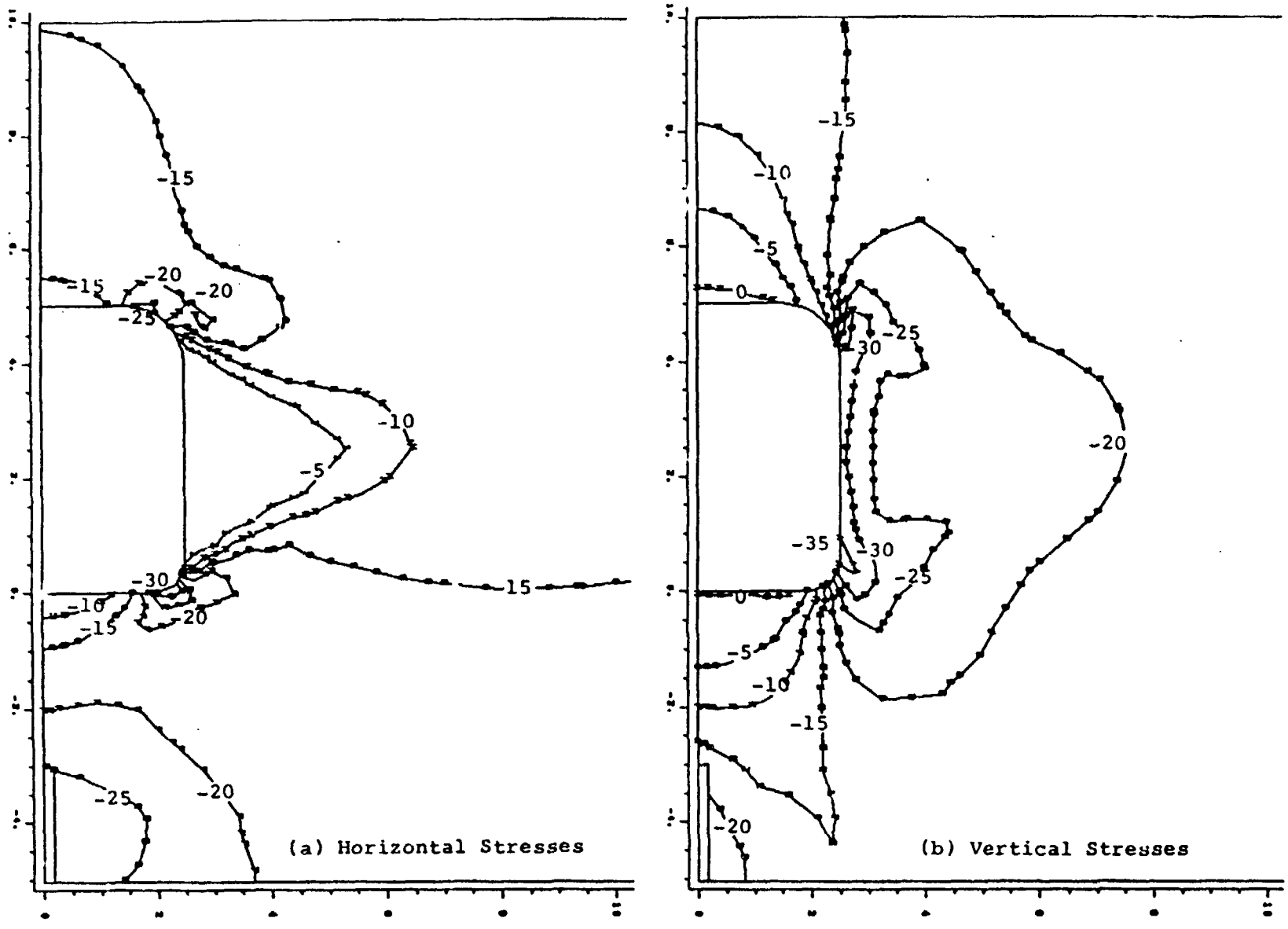

Figure 34. Horizontal and Vertical Stress Contours 5 Years After Emplacement for HLW, GTL = 100 kw/A, Boiling at 100°C.

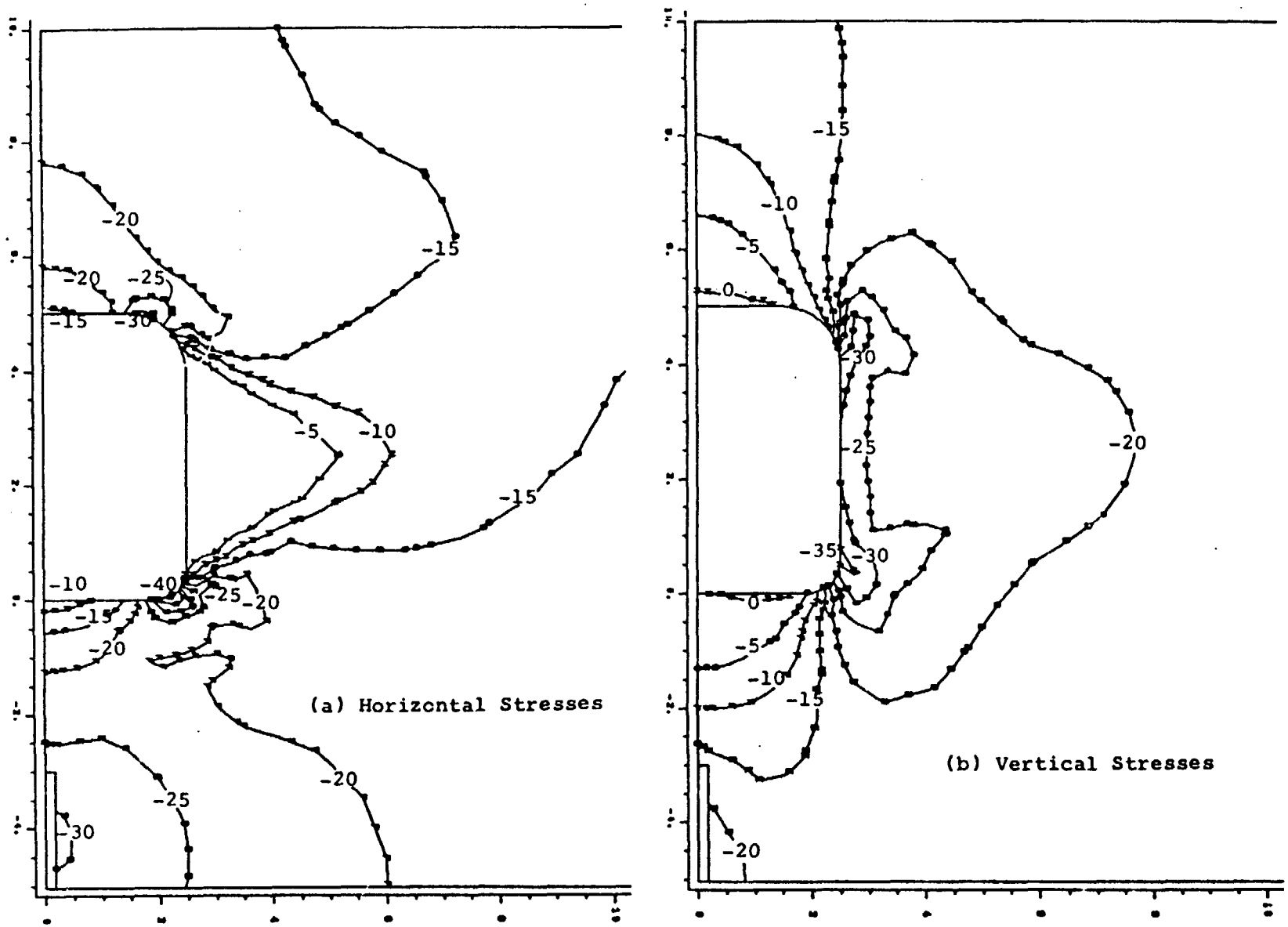

Figure 35. Horizontal and Vertical Stress Contours 10 Years After Emplacement for HLW, GTL = 100 kw/A, Boiling at 100°C.

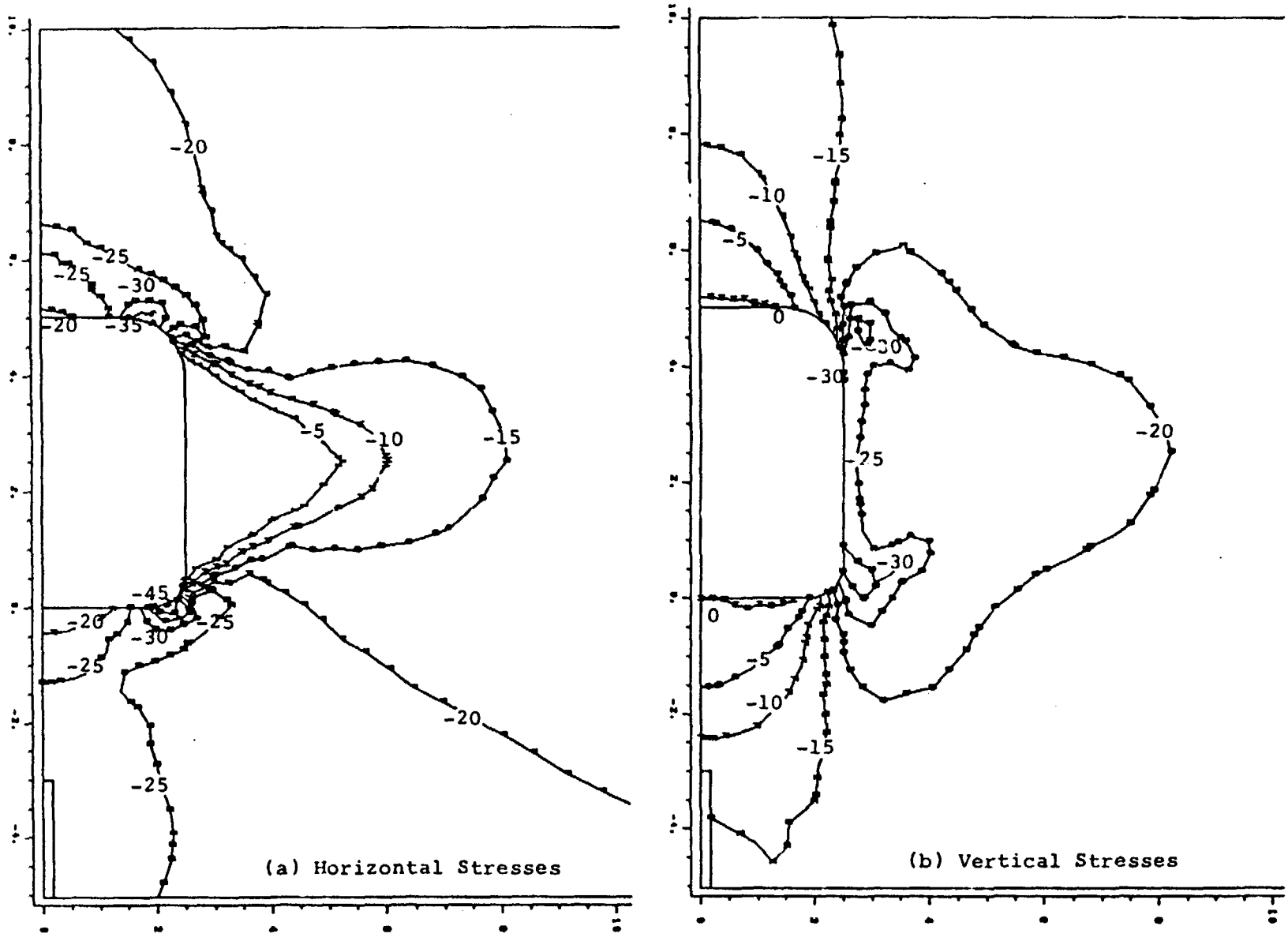

Figure 36. Horizontal and Vertical Stress Contours 50 Years After Emplacement for HLW, GTL = 100 kw/A, Boiling at 100°C.

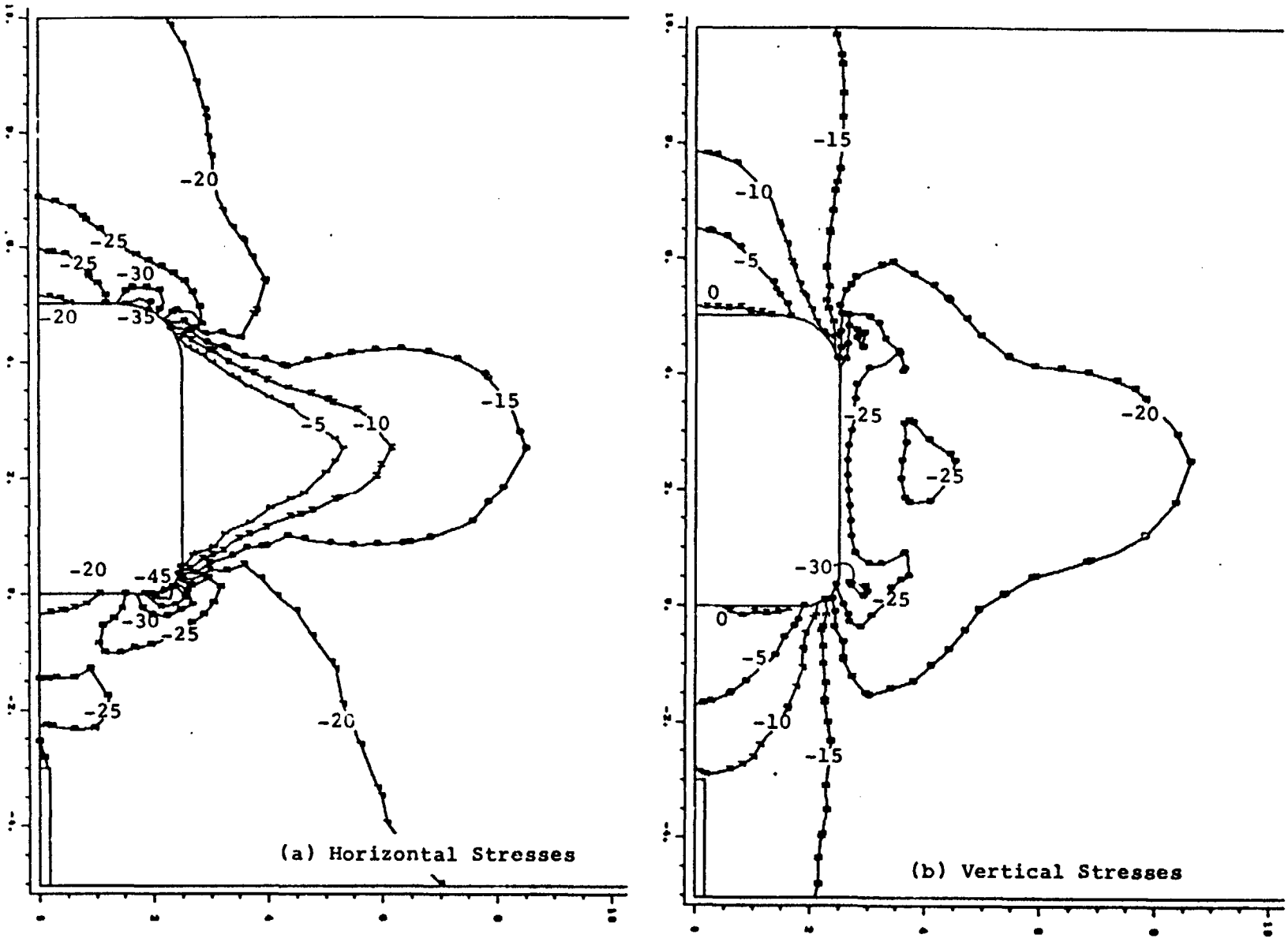

Figure 37. Horizontal and Vertical Stress Contours 100 Years After Emplacement for HLW, GTL = 100 kw/A, Boiling at 100°C.

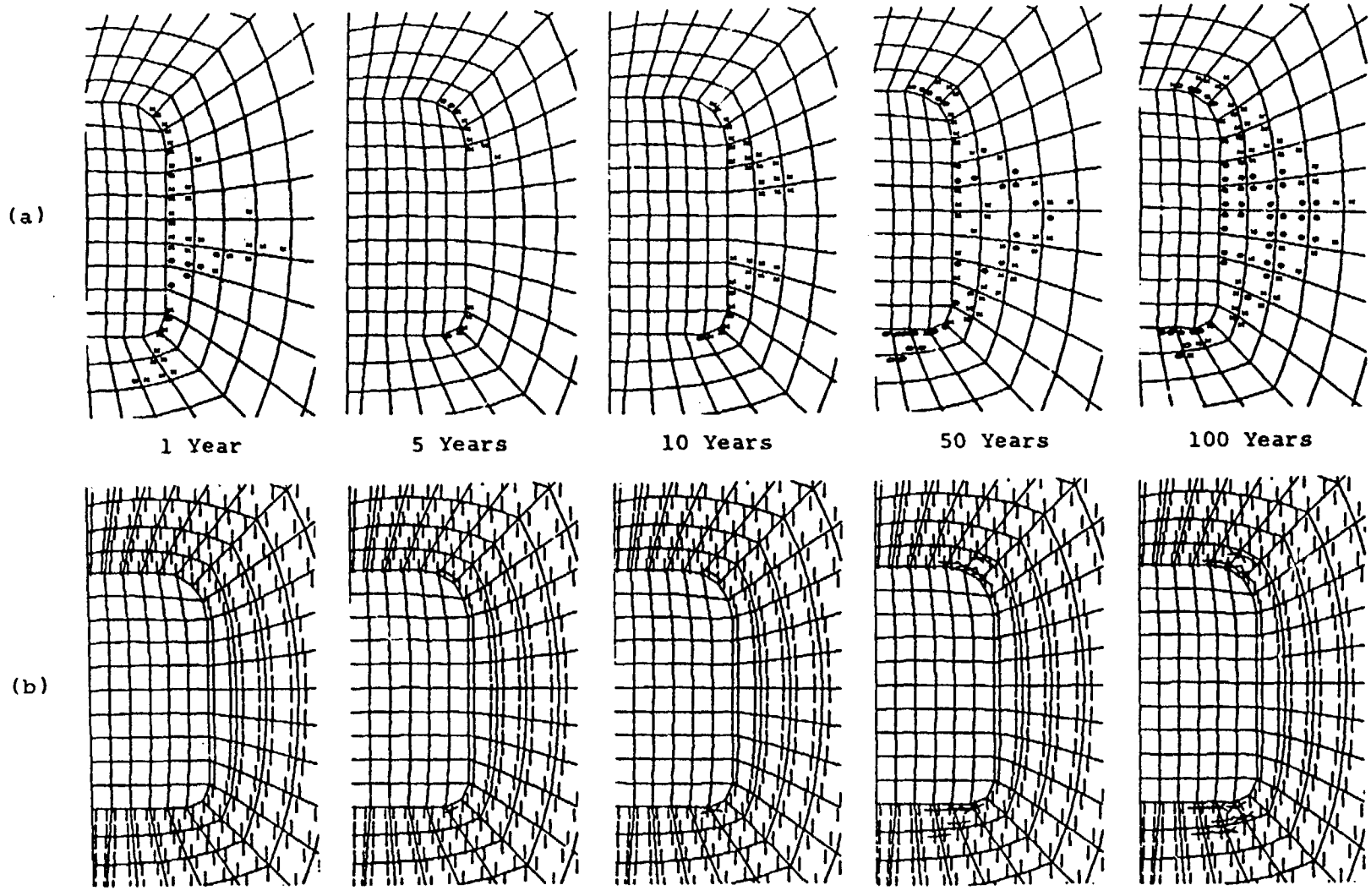

Figure 38. (a) Joint State Indicators at Various Times;
(b) Joint and Crack Orientations at Various Times
for HLW, GTL = 100 kw/A, No Boiling of Groundwater

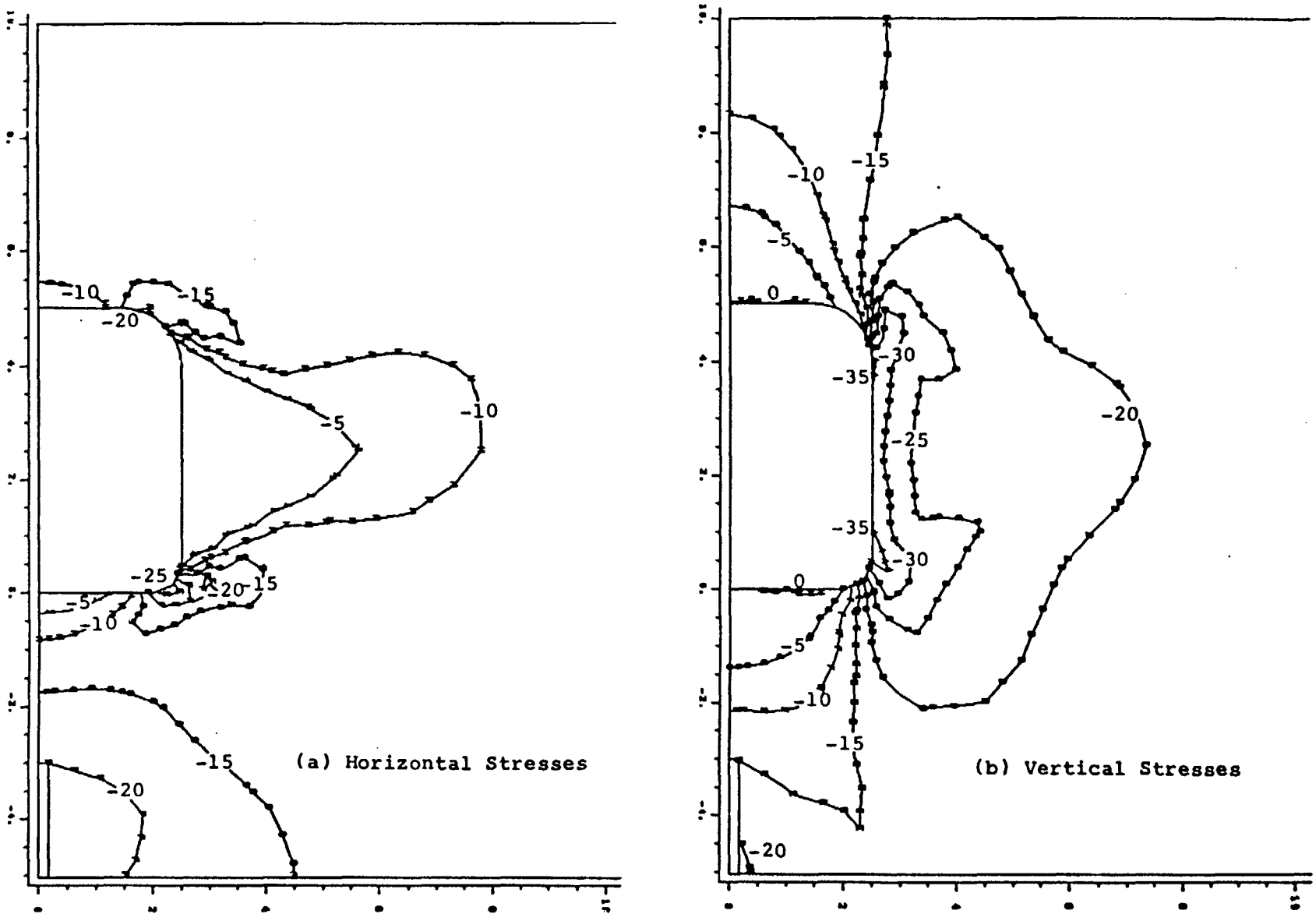

Figure 39. Horizontal and Vertical Stress Contours 1 Year After Emplacement for HLW, GTL = 100 kw/A, No Boiling of Groundwater.

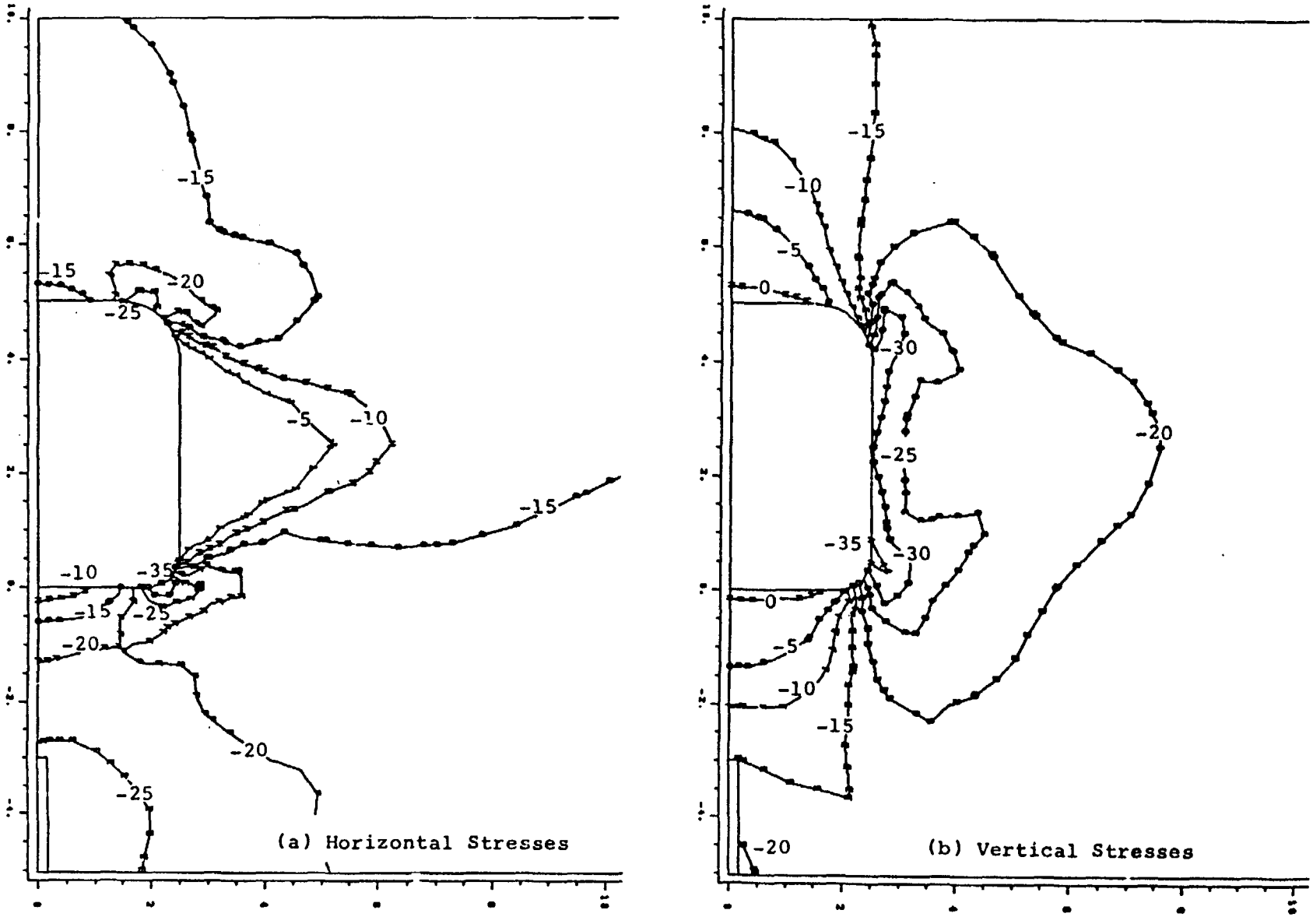

Figure 40. Horizontal and Vertical Stress Contours 5 Years After Emplacement for HLW, GTL = 100 kw/A, No Boiling of Groundwater.

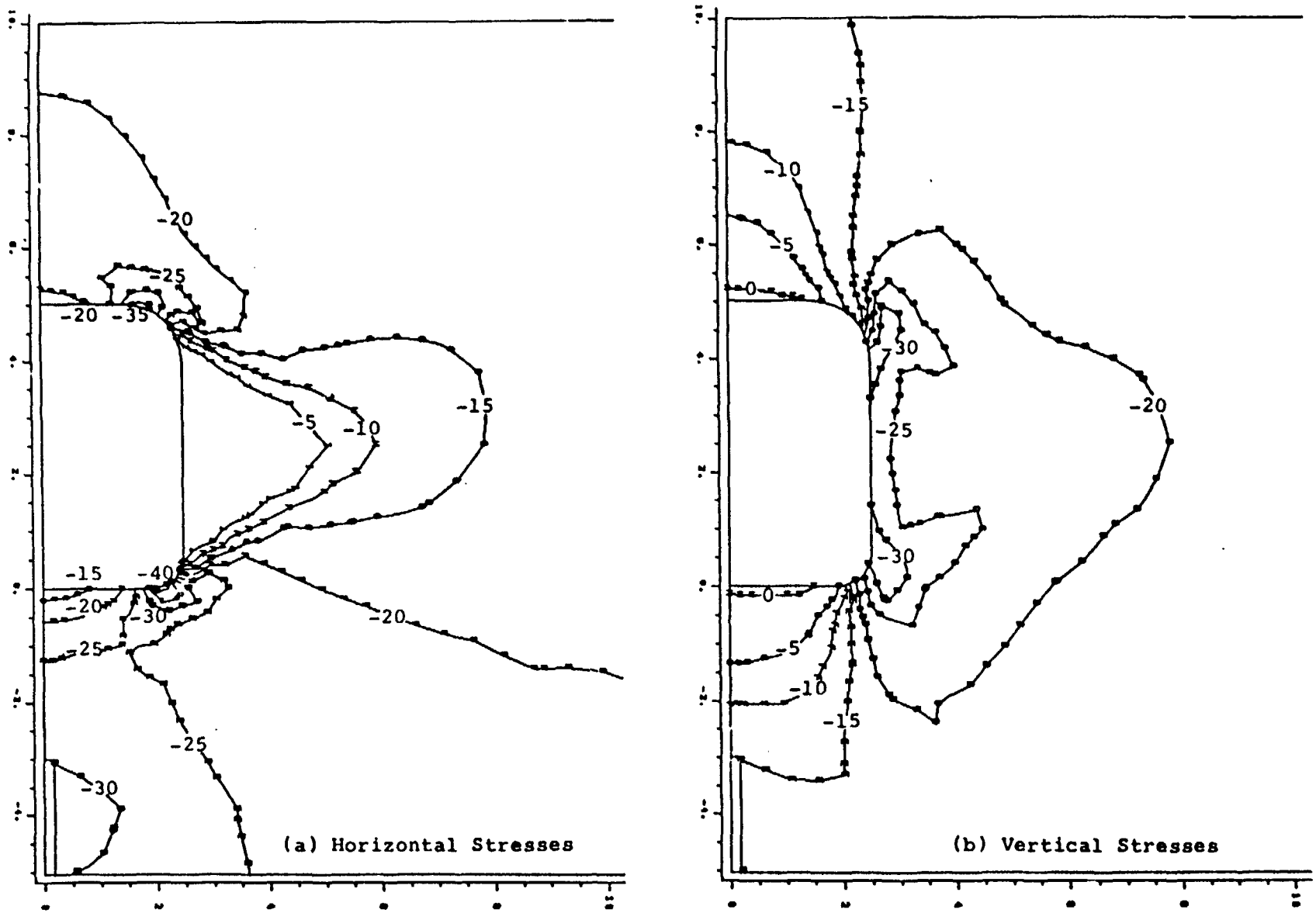

Figure 41. Horizontal and Vertical Stress Contours 10 Years After Emplacement for HLW, GTL = 100 kw/A, No Boiling of Groundwater.

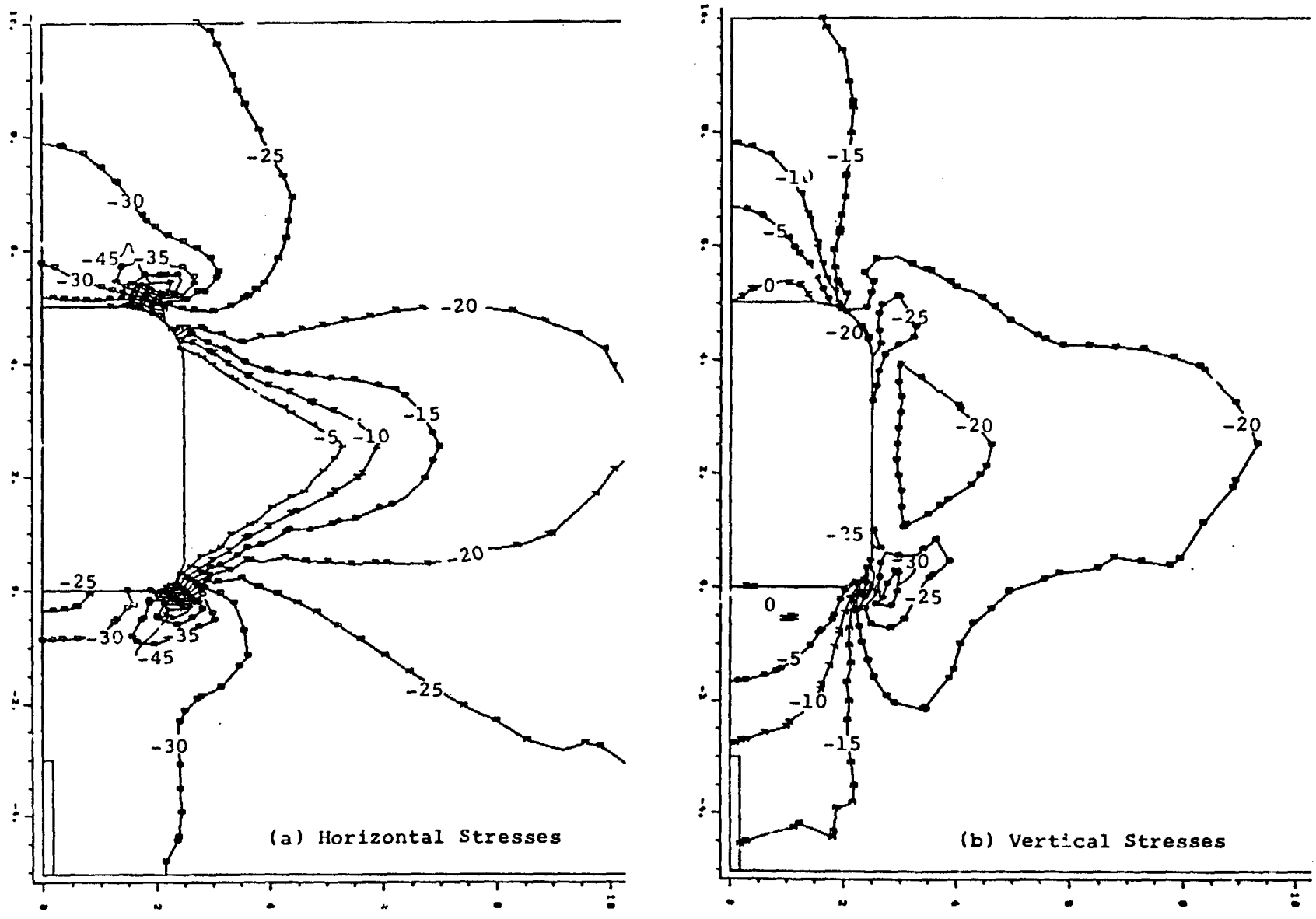

Figure 42. Horizontal and Vertical Stress Contours 50 Years After Emplacement for HLW, GTL = 100 kw/A, No Boiling of Groundwater.

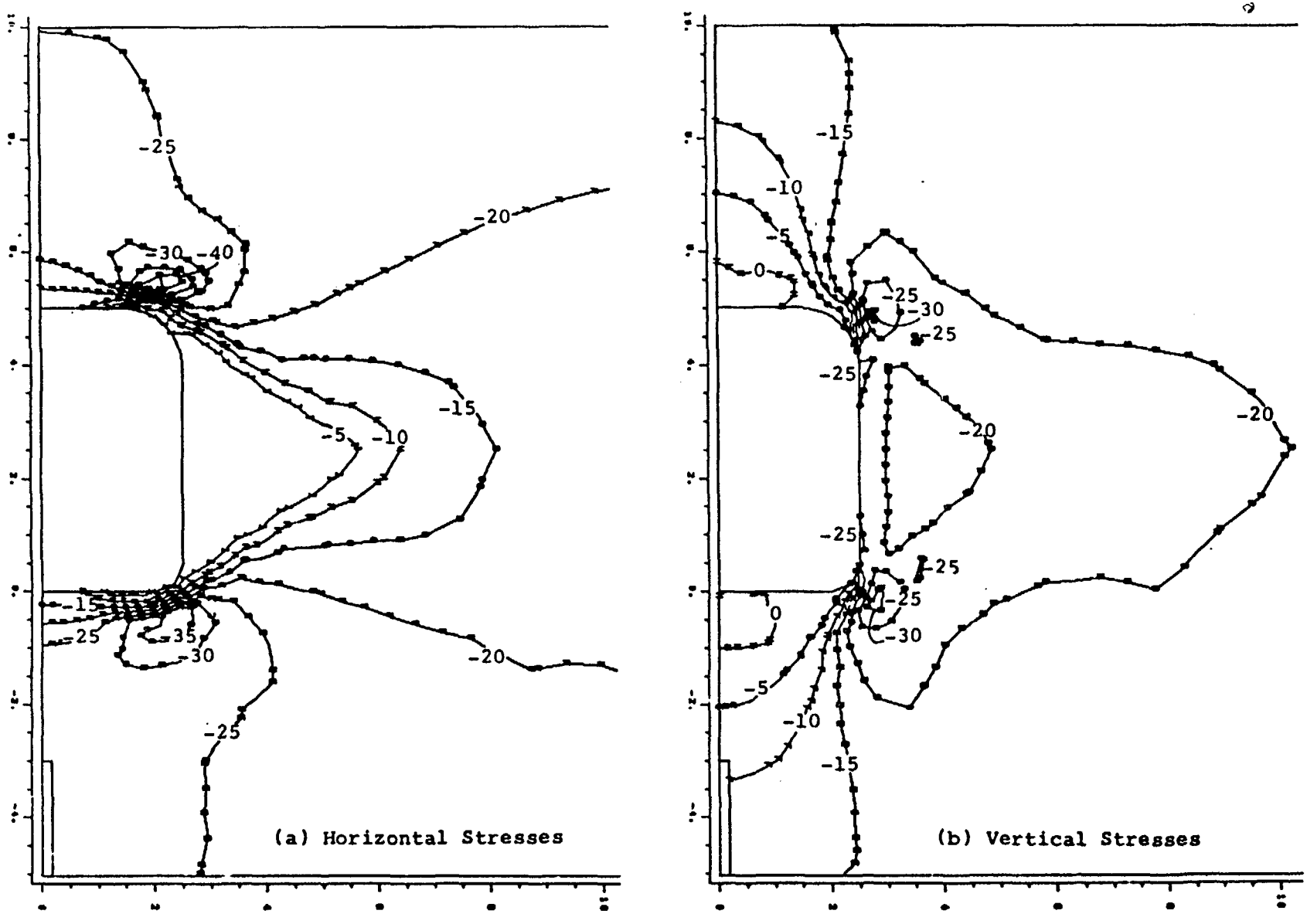

Figure 43. Horizontal and Vertical Stress Contours 100 Years After Emplacement for HLW, GTL = 100 kw/A, No Boiling of Groundwater.

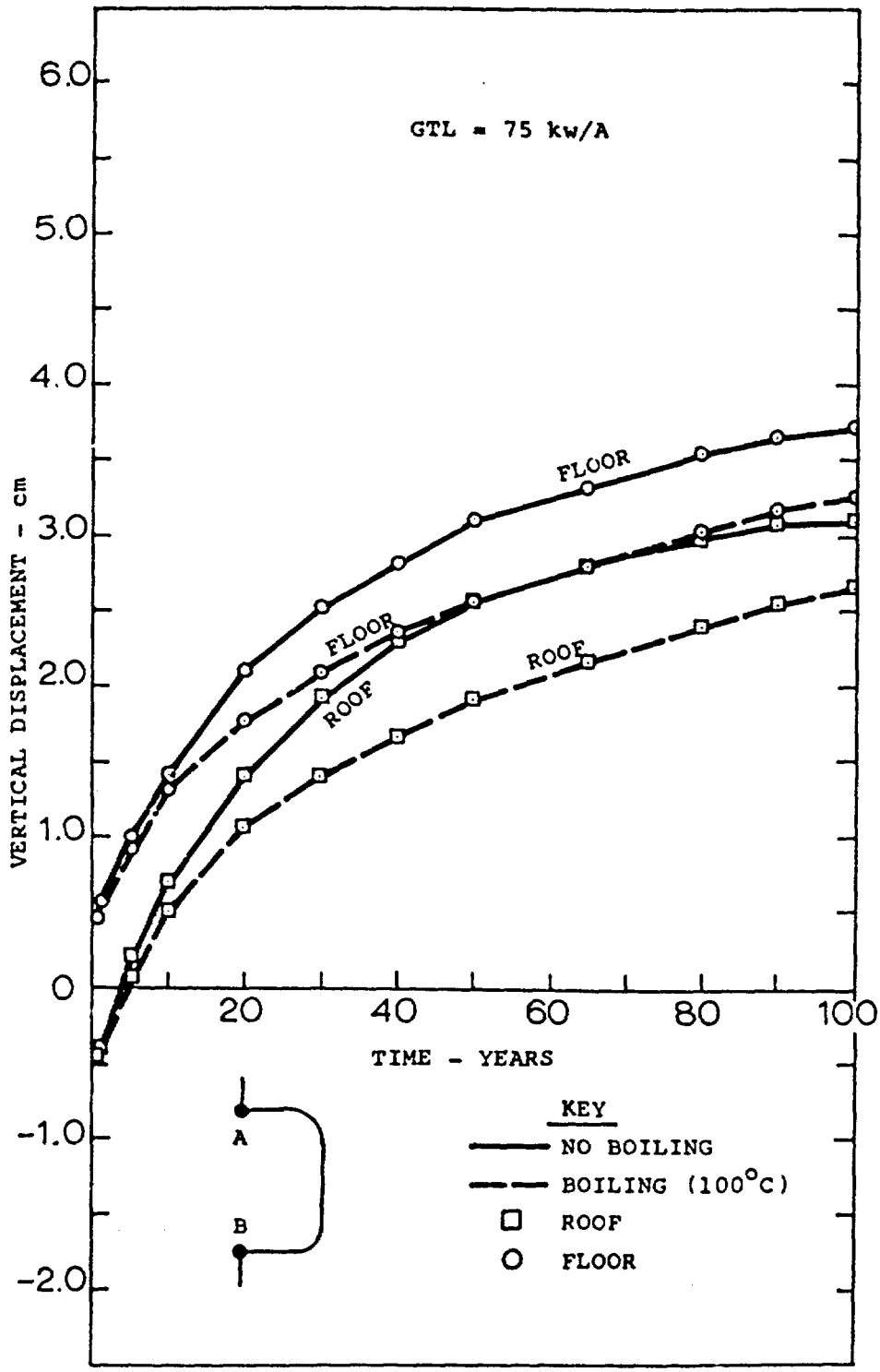

Figure 44. Displacements of Room at Centerline of Floor and Roof for HLW, GTL = 75 kw/A, Boiling and No Boiling Conditions.

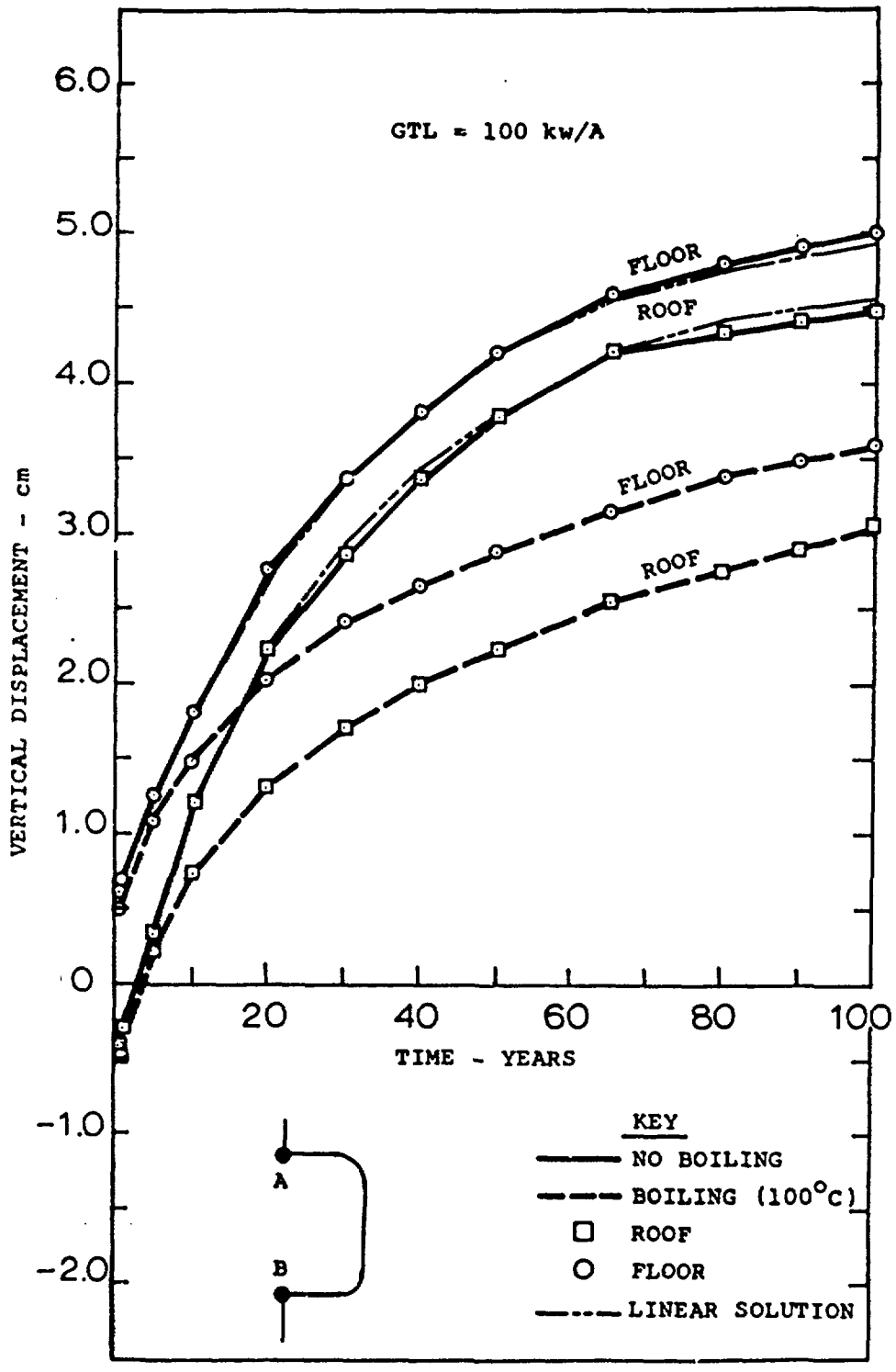

Figure 45. Displacements of Room at Centerline of Floor and Roof for HLW, GTL = 100 kw/A, Boiling and No Boiling Conditions.

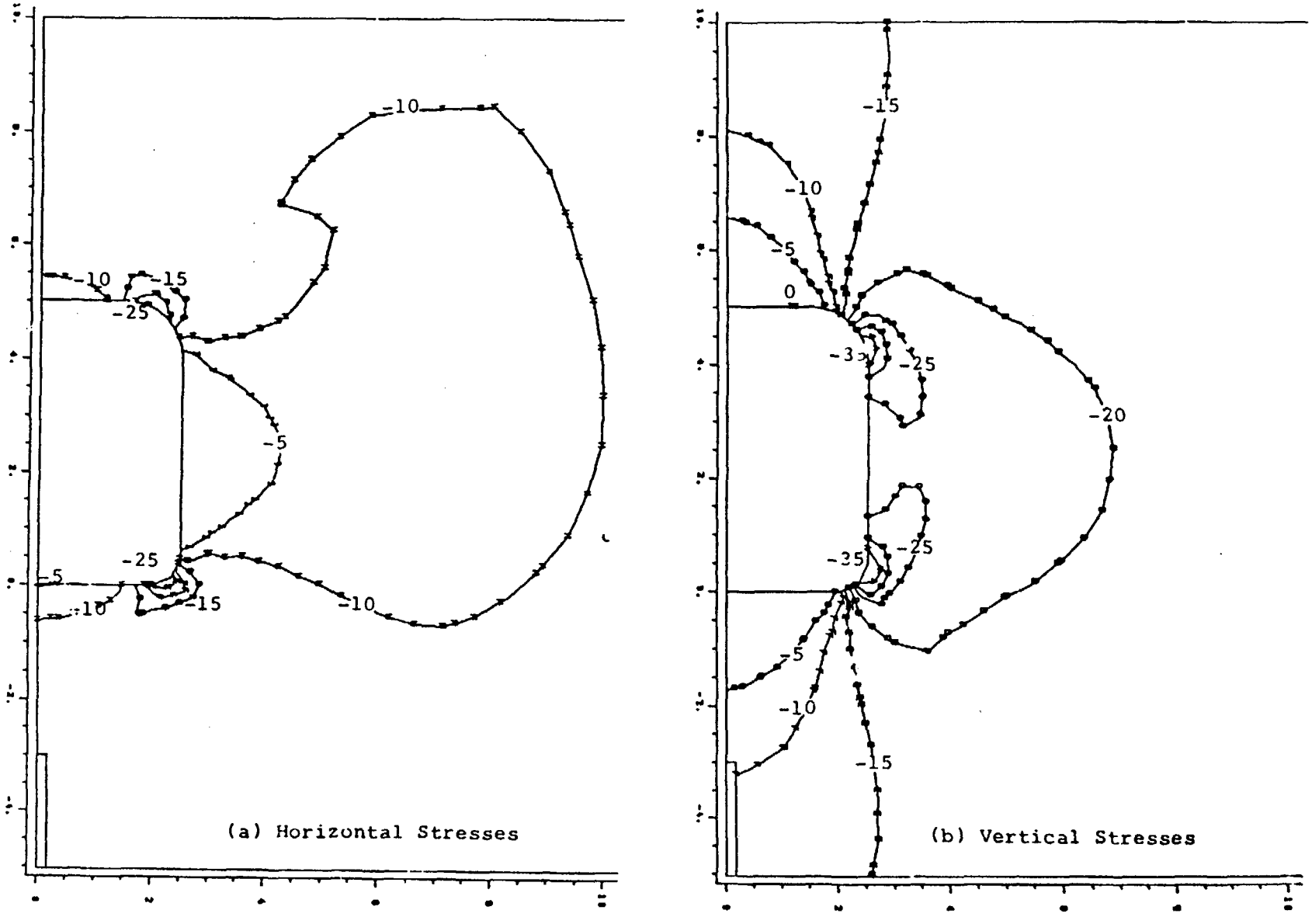

Figure 46. Horizontal and Vertical Stress Contours After Excavation for HLW, GTL = 100 kw/A, Linear Solution, No Boiling.

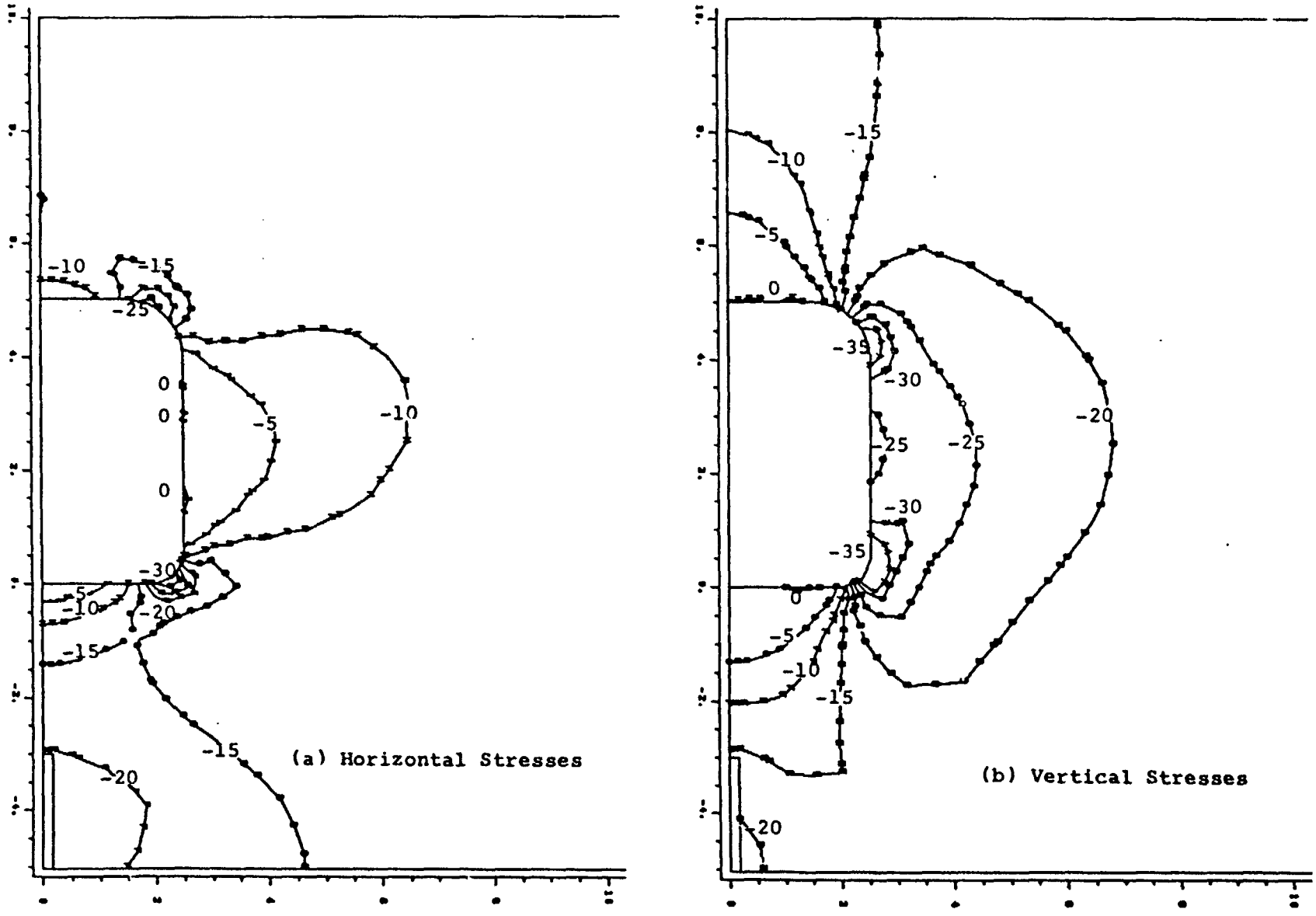

Figure 47. Horizontal and Vertical Stress Contours 1 Year After Emplacement for HLW, GTL = 100 kw/A, Linear Solution, No Boiling of Groundwater.

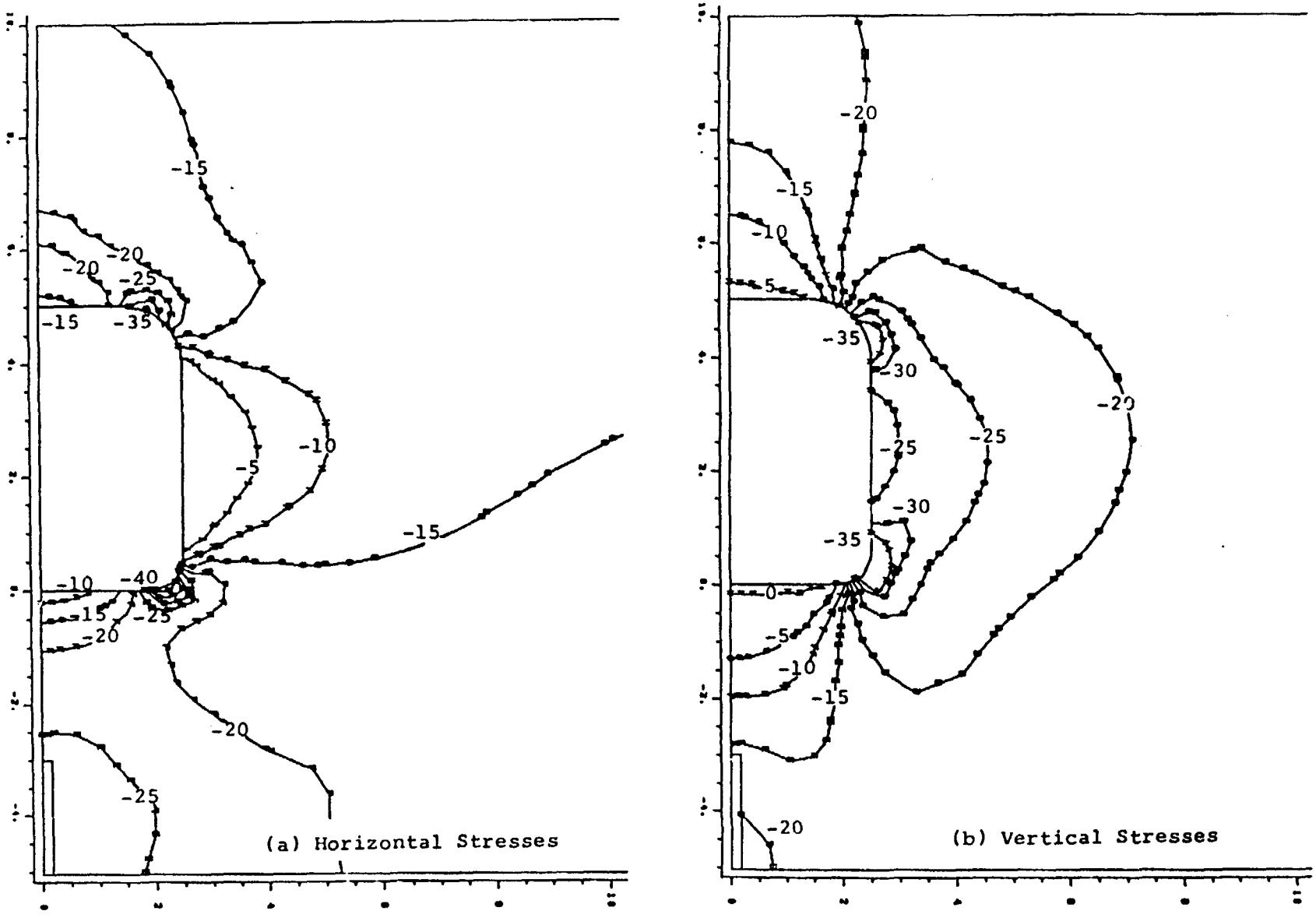

Figure 48. Horizontal and Vertical Stress Contours 5 Years After Emplacement for HLW, GTL = 100 kw/A, Linear Solution, No Boiling of Groundwater.

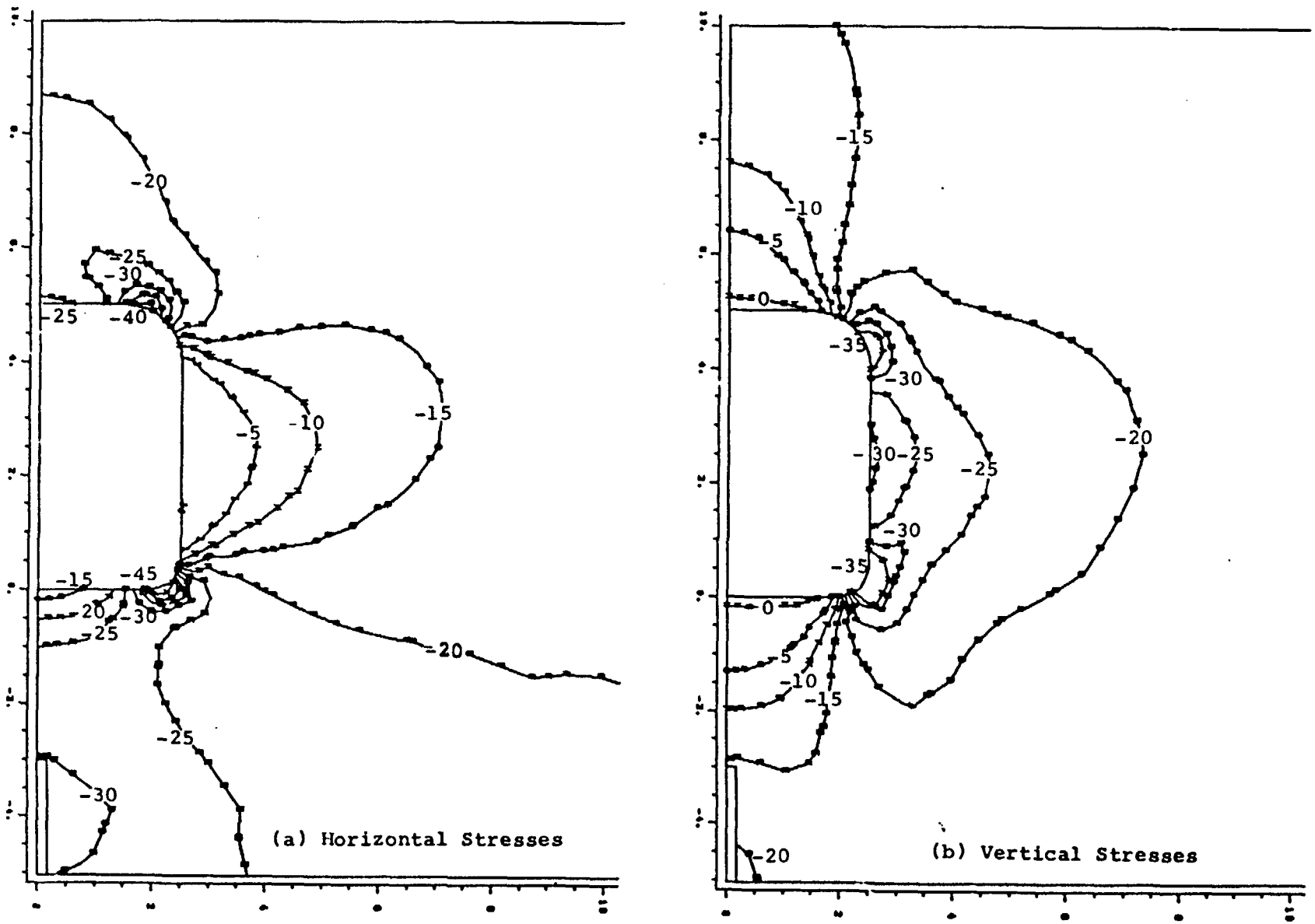

Figure 49. Horizontal and Vertical Stress Contours 10 Years After Emplacement for HLW, GTL = 100 kw/A, Linear Solution, No Boiling of Groundwater.

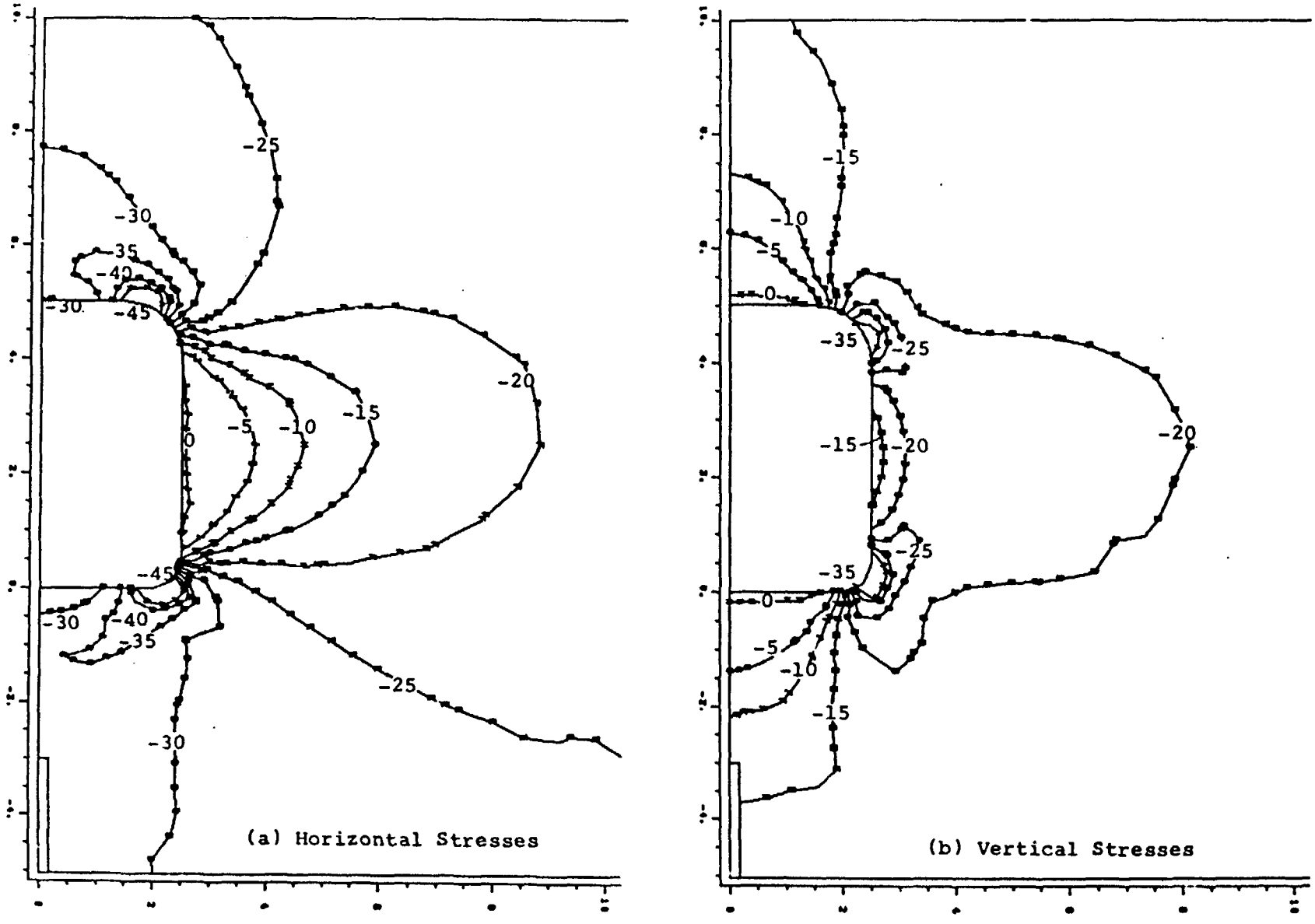

Figure 50. Horizontal and Vertical Stress Contours 50 Years After Emplacement for HLW, GTL = 100 kw/A, Linear Solution, No Boiling of Groundwater.

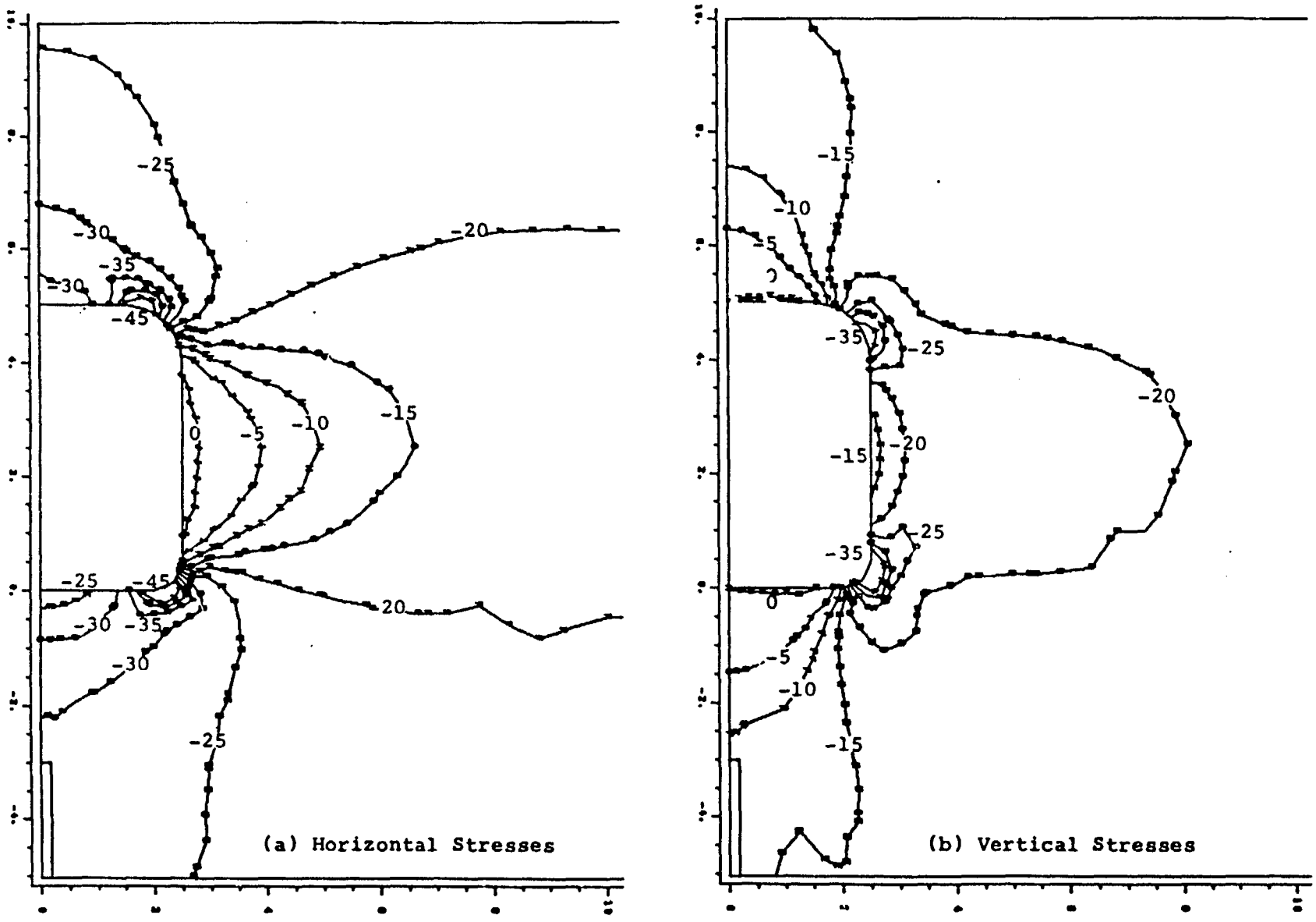

Figure 51. Horizontal and Vertical Stress Contours 100 Years After Emplacement for HLW, GTL = 100 kw/A, Linear Solution, No Boiling of Groundwater.

Distribution:

C. A. Heath, Director
Office of Waste Isolation
U. S. Department of Energy
Room B-207
Germantown, MD 20767

D. L. Vieth, Acting Team Leader
Technology Team
U. S. Department of Energy
Room B-220
Germantown, MD 20767

J. O. Neff, Program Manager
National Waste Terminal
Storage Program Office
U. S. Department of Energy
505 King Avenue
Columbus, OH 43201

L. D. Ramspott
Technical Project Officer
Lawrence Livermore National
Laboratory
University of California
P. O. Box 808
Mail Stop L-204
Livermore, CA 94550

B. R. Erdal
Technical Project Officer
Los Alamos National Laboratory
University of California
P. O. Box 1663
Mail Stop 514
Los Alamos, NM 87545

A. R. Hakl, Site Manager
Westinghouse - AESD
P. O. Box 708
Mail Stop 703
Mercury, NV 89023

G. L. Dixon
Technical Project Officer
U. S. Geological Survey
P. O. Box 25046
Mail Stop 954
Federal Center
Denver, CO 80301

W. E. Wilson
U. S. Geological Survey
P. O. Box 25046
Mail Stop 954
Denver, CO 80301

W. S. Twenhofel
820 Estes Street
Lakewood, CO 80226

C. R. Cooley, Deputy Director
Office of Waste Isolation
U. S. Department of Energy
Room B-214
Germantown, MD 20767

R. G. Goranson
U. S. Department of Energy
Richland Operations Office
P. O. Box 550
Richland, WA 99352

R. Deju
Rockwell International Atomics
International Division
Rockwell Hanford Operations
Richland, WA 99352

R. M. Nelson, Jr., Dir. (3)
Waste Management Project Office
U. S. Department of Energy
P. O. Box 14100
Las Vegas, NV 89114

D. F. Miller, Director
Office of Public Affairs
U. S. Department of Energy
P. O. Box 14100
Las Vegas, NV 89114

R. H. Marks
U. S. Department of Energy
CP-1, M/S 210
P. O. Box 14100
Las Vegas, NV 89114

B. W. Church, Director
Health Physics Division
U. S. Department of Energy
P. O. Box 14100
Las Vegas, NV 89114

R. R. Loux (7)
U. S. Department of Energy
P. O. Box 14100
Las Vegas, NV 89114

A. E. Gurrola
Holmes & Narver, Inc.
P. O. Box 14340
Las Vegas, NV 89114

K. Street, Jr.
Lawrence Livermore National Laboratory
University of California
Mail Stop L-209
P. O. Box 808
Livermore, CA 94550

D. C. Hoffman
Los Alamos National Laboratory
Mail Stop 760
P. O. Box 1663
Los Alamos, NM 87545

N. E. Carter
Battelle
Office of Nuclear Waste Isolation
505 King Avenue
Columbus, OH 43201

W. A. Carbiener
Battelle
Office of NWTS Integration
505 King Avenue
Columbus, OH 43201

S. Goldsmith
Battelle
Office of Nuclear Waste Isolation
505 King Avenue
Columbus, OH 43201

ONWI Library (5)
Battelle
Office of Nuclear Waste Isolation
505 King Avenue
Columbus, OH 43201

R. M. Hill
State Planning Coordinator
Governor's Office of Planning Coordination
State of Nevada
Capitol Complex
Carson City, NV 89023

N. A. Clark
Department of Energy
State of Nevada
Capitol Complex
Carson City, NV 89710

J. P. Colton
International Atomic Energy Agency
Div. of Nuclear Power & Reactors
P. O. Box 590, A-1011
Vienna, Austria

H. D. Cunningham
Reynolds Electrical & Engineering Company, Inc.
Mail Stop 555
P. O. Box 14400
Las Vegas, NV 89114

J. A. Cross
Fenix & Scisson, Inc.
P. O. Box 15408
Las Vegas, NV 89114

A. M. Friedman
Argonne National Laboratories
9700 S. Cass Avenue
Argonne, IL 60439

1417	F. W. Muller
3141	L. J. Erickson (5)
3151	W. L. Garner (3)
3154-3	C. H. Dalin (25) (For DOE/TIC)
4530	R. W. Lynch
4531	L. W. Scully
4537	L. D. Tyler
4537	B. S. Langkopf
4537	A. R. Lappin
4537	R. M. Zimmerman
4537	R. Shaw
4538	R. C. Lincoln
4538	A. E. Stephenson
5500	O. E. Jones
5510	D. B. Hayes
5511	J. W. Nunziato
5511	D. K. Gartling
5520	T. B. Lane
5521	N. E. Gilbertsen
5521	C. M. Stone
5521	R. K. Thomas
5522	R. L. Johnson
5524	L. W. Davison
5530	W. Herrmann
5531	M. L. Blanford
5532	B. M. Butcher
5532	W. A. Olsson
5541	W. C. Luth
8266	E. A. Aas